

Deep Inelastic Scattering on an Extremal RN-AdS Black Hole II: Holographic Fermi Surface

Kiminad A. Mamo^{*} and Ismail Zahed[†]

Department of Physics and Astronomy, Stony Brook University, Stony Brook, New York 11794-3800, USA

(Dated: December 4, 2019)

We consider deep inelastic scattering (DIS) on a dense nucleus described as an extremal RN-AdS black hole with holographic quantum fermions in the bulk. We evaluate the 1-loop fermion contribution to the R-current on the charged black hole, and map it on scattering off a Fermi surface of a dense and large nucleus with fixed atomic number. Near the black hole horizon, the geometry is that of $\text{AdS}_2 \times \text{R}^3$ where the fermions develop an emergent Fermi surface with anomalous dimensions. DIS scattering off these fermions yields to anomalous partonic distributions mostly at large- x , as well as modified hard scattering rules. The pertinent R-ratio for the black hole is discussed. For comparison, the structure functions and the R-ratio in the probe or dilute limit with no back-reaction on the geometry, are also derived. We formulate a hybrid holographic model for DIS scattering on heavy and light nuclei, which compares favorably to the existing data for Pb, Au, Fe, C and He over a wide range of parton- x .

PACS numbers:

I. INTRODUCTION

Many years ago the EMC collaboration at CERN has revealed that DIS scattering on an iron nucleus deviates substantially from deuterium [1] contrary to established lore. Since then, many other collaborations using both electron and muon probes have confirmed this observation [2–4]. Although the nucleus is a collection of loosely bound nucleons with confined quarks, DIS scattering is much richer in a nucleus. The nuclear structure functions display shadowing at low- x , a depletion at intermediate- x , and an enhancement due mostly to Fermi motion at large- x .

QCD supports the idea that hadrons are composed of quarks and gluons as revealed by DIS scattering of electrons on nucleons at SLAC. The scaling laws initially reported follows from scattering on point-like object or partons. Because of asymptotic freedom, the partons interact weakly at short distances leading to relatively small scaling violations at intermediate- x . At low- x , perturbative QCD predicts a large enhancement in the nucleon structure functions due to the rapid growth of the gluons [5] that eventually saturate [6]. This observation has been confirmed at HERA [7, 8].

DIS in holography at moderate- x is different from weak coupling as it involves hadronic and not partonic constituents [9]. The large gauge coupling causes the charges to rapidly deplete their energy and momentum, making them invisible to hard probes. However, because the holographic limit enjoys approximate conformal symmetry, the form factors exhibit various scaling laws including the parton-counting rules [10]. The holographic structure functions fail to reproduce the Callan-Gross sum rule [9]

at intermediate- x , but agree with it at large- x when the parton momentum fraction neighbors 1 [11]. In contrast, DIS scattering at low- x on a non-extremal thermal black-hole was argued to be partonic and fully saturated [12].

This paper is a follow up on our recent investigation of DIS scattering on a nucleus as an extremal RN-AdS black hole [13]. In the double limit of a large number of colors and gauge coupling, the leading contribution amounts to the Abelian part of the R-current being absorbed in bulk by the black-hole. After mapping at the boundary, the ensuing nuclear structure functions show strong shadowing at low- x , but wane exponentially for large- x as originally noted for the thermal black hole in [12].

At next to leading-order, the R-current scatters off charged fermionic pairs forming a holographic Fermi liquid around the black hole. The purpose of this paper is to detail DIS scattering on this dense holographic liquid as the analogue of DIS scattering on a nucleus described as a Fermi liquid. Some aspects of this liquid near the horizon were initially discussed in lower dimensions [14]. It should be noted that at next to leading order the R-current scatters also off bulk charged scalars. However, these scalars are bosonic and do not form a Fermi surface. Their contribution will not be considered in this work.

Standard DIS scattering on a nucleus is mostly on a Fermi gas in a mean field "trap", so the present calculations show how the same scattering operates on an emergent Fermi surface with strongly coupled fermionic constituents in a "trap" produced by a charged black-hole. A chief observation is that the partonic structure functions at large- x , are modified by an emergent Fermi surface. The latter follows from an $\text{AdS}_2 \times \text{R}^3$ reduction of the geometry near the black-hole horizon, and asymptotes a warped Fermi liquid near the boundary. The corresponding R-ratio exhibits shadowing at very low- x , anti-shadowing at intermediate- x and Fermi motion at large- x , much like the R-ratio for DIS scattering on finite

^{*}Electronic address: kiminad.mamo@stonybrook.edu

[†]Electronic address: ismail.zahed@stonybrook.edu

nuclei. Shadowing is caused by the coherent many-body effects and is captured by DIS scattering in leading order on the black-hole at low- x , while Fermi motion at large- x is due to the incoherent scattering on quantum fermions around the black hole in the form of a holographic Fermi surface.

This paper consists of several new results: 1/ an explicit derivation of the structure functions for DIS scattering on the emerging holographic Fermi surface around an extremal black hole; 2/ the characterization of these structure functions both at large- x and low- x , with the identification of new anomalous exponents at large x ; 3/ an explicit derivation of the R-ratio for DIS scattering on the extremal black hole as a model for DIS scattering on a dense and finite nucleus; 4/ an explicit derivation of the same structure functions in the probe fermion limit as a model for DIS scattering on a dilute nucleus; 5/ a comparative study of the R-ratio in the probe limit.; 6/ a detailed comparison to the empirical DIS scattering data from light to heavy nuclei.

The organization of the paper is as follows: in section II, we briefly review the setting for the extremal RN-AdS black hole, and the key characteristics of the holographic Fermi liquid. In section III, we derive the contribution to the boundary effective action of an R-photon scattering off bulk quantum fermions. The result is quantum and dominant at large- x , and corrects the classical and leading contribution from the bulk black hole. In section IV, we analyze the contribution stemming from the quantum fermions near the horizon. In section V, we detail our derivation of the R-ratio for DIS scattering on a dense nucleus as quantum corrected holographic black hole. For comparison, we discuss in section VI the probe or dilute limit with the bulk fermions carrying a finite density in AdS without affecting the underlying geometry. The pertinent R-ratio in this regime is derived and analyzed. In section VII we motivate a hybrid holographic model for DIS scattering on light and heavy nuclei which compares favorably to the existing world-data for a wide range of parton- x . Our conclusions are in section VIII. Some useful details are found in several Appendices.

II. EXTREMAL BLACK HOLE : DENSE LIMIT

In this work we will address DIS scattering on a cold and dense nucleus as a dual to an RN-AdS black hole following on our recent analysis [18]. Conventional DIS scattering on cold nuclei with many of the conventions used are reviewed in [19]. In holography, DIS scattering on a nucleus as an RN-AdS black hole is illustrated in Fig. 1. In the holographic limit, the leading contribution is Fig. 1a with the structure functions being the absorbed parts of the R-current. To this order, the structure functions have considerable support mostly at low- x [13] (see below). At next-to-leading order, the R-current is absorbed through the virtual fermionic loop shown in Fig. 1b. This loop describes a fermionic hallow

around the RN-AdS black hole that acts as a holographic Fermi liquid. Below we detail how this contribution leads to structure functions with mostly support at large- x . This description is complementary to our recent analysis based on a generic density expansion around a trapped Fermi liquid [18].

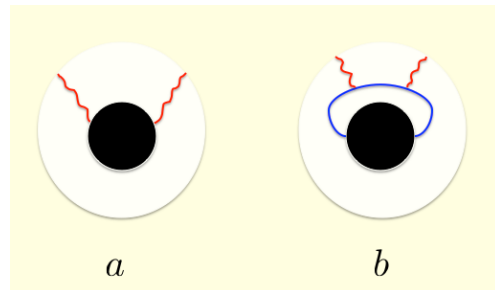


FIG. 1: Absorptive part of the R-current on a nucleus as an extremal RN-AdS black hole: (a) absorptive contribution to order N_c^2 ; (b) absorptive fermionic contribution to order N_c^0 .

A. The extremal and charged black hole

The RN-AdS black hole is described by effective gravity coupled to a U(1) gauge field in a 5-dimensional curved AdS space [15]

$$S = \frac{1}{2\kappa^2} \int d^5x \sqrt{-g} (\mathbb{R} - 2\Lambda) - \frac{1}{4e^2} \int d^5x \sqrt{-g} F^2 \quad (\text{II.1})$$

The Ricci scalar is \mathbb{R} , and $\kappa^2 = 8\pi G_5$ and $\Lambda = -6/R^2$ are the gravitational and cosmological constant. The curvature radius of the AdS space is R with line element

$$ds^2 = \frac{r^2}{R^2} (-f dt^2 + d\vec{x}^2) + \frac{R^2}{r^2 f} dr^2 \quad (\text{II.2})$$

and warping factor

$$f(r) = \left(1 - \frac{r_+^2}{r^2}\right) \left(1 - \frac{r_-^2}{r^2}\right) \left(1 + \frac{r_+^2}{r^2} + \frac{r_-^2}{r^2}\right) \quad (\text{II.3})$$

with $r_+ > r_-$ the outer-inner horizons satisfying $f(r_\pm) = 0$.

The black-hole is charged and sources the R-potential

$$A_t = \mu - \frac{Q}{r^2} \quad (\text{II.4})$$

provided that the electric charge Q and the geometrical charge q satisfy

$$\frac{q^2 R^2}{Q^2} = \frac{4}{3} \times \frac{2\kappa^2}{4e^2} = \frac{R^2}{6\tilde{\alpha}}, \quad (\text{II.5})$$

where

$$\begin{aligned} 2\kappa^2 &= \frac{8\pi^2 R^3}{N_c^2} \\ 4e^2 &= \tilde{\alpha} \frac{64\pi^2 R}{N_c^2} \end{aligned} \quad (\text{II.6})$$

We have defined $\tilde{\alpha} = 1$ for a U(1) R-charge, and $\tilde{\alpha} = \frac{1}{4} \frac{N_c}{N_f}$ for a D3-D7 U(1) vector charge. The temperature of the RN-AdS black hole is

$$T = \frac{r_+^2 f'(r_+)}{4\pi R^2} = \frac{r_+}{\pi R^2} \left(1 - \frac{\mu^2 \pi^2 R^4 \gamma^2}{r_+^2}\right) \quad (\text{II.7})$$

with $\gamma^2 = 1/12\pi^2 \tilde{\alpha}$. The chemical potential μ is fixed by the zero potential condition on the outer horizon $A_t(r_+) = 0$ or $\mu = Q/r_+^2$. At extremality where $T = 0$, we have $r_+ = r_- = \pi R^2 \gamma \mu = \frac{R^2}{2\sqrt{3}} \sqrt{\tilde{\alpha}}$.

B. Holographic Fermi liquid

The fermionic fields in bulk are characterized by the Dirac action in a charged AdS black hole geometry

$$S = - \int d^5x \sqrt{-g} i(\bar{\psi} \Gamma^M \mathcal{D}_M \psi - m \bar{\psi} \psi) \quad (\text{II.8})$$

with $\bar{\psi} = \psi^\dagger \Gamma^t$, and the long derivative

$$\mathcal{D}_M = \partial_M + \frac{1}{4} \omega_{abM} \Gamma^{ab} - ie_R A_M \quad (\text{II.9})$$

The indices $M, N \dots$ or $\mu, \nu, r \dots$ refer to the space-time indices, and a, b, \dots to space-time indices with underline correspond to tangent space indices. Therefore, for example, Γ^a denotes the gamma matrices in the tangent space, Γ^M denotes gamma matrices in the curved space-time. They are specifically given in Appendix A.

A bulk fermion field of mass m and R-charge e_R is dual to a composite boundary field of conformal dimension $\Delta = \frac{3}{2} + mR$. Since the horizon of the extremal charged RN-AdS black is characterized by a finite U(1) electric field, fermionic pair creation takes place through the Schwinger mechanism. As a result, the black-hole say with positive R-charge absorbs the negative part of the pairs and expel the positive part. Since AdS is hyperbolic and confining, the positive charge falls back to the surface of the black hole, accumulating into a hallow or holographic Fermi liquid.

The characteristics of the low-lying excitations of the holographic Fermi liquid for low frequencies $|k^0| < \mu$ and low momenta $k = |\vec{k}|$, have been discussed in [16, 17]. In particular, near the horizon the AdS₅ geometry factors into AdS₂ × R³.

Case-1: $e_R^2 \tilde{\alpha} < \frac{1}{4}(mR)^2$

The fermions exhibit strong distorsion in the AdS₂ geometry, with [16]

$$\mathcal{G}_R^{11}(k^0, \vec{k}) = C(\vec{k}) (k^0)^{2\nu_k} \begin{pmatrix} 0 & 0 \\ 0 & 1 \end{pmatrix}, \quad (\text{II.10})$$

and

$$\begin{aligned} \nu_k &= \frac{\sqrt{\tilde{\alpha}}}{\mu} (k^2 - k_R^2)^{\frac{1}{2}} \\ &\equiv \frac{\sqrt{\tilde{\alpha}}}{\mu} \left(k^2 - \frac{\mu^2}{3\tilde{\alpha}} \left(e_R^2 \tilde{\alpha} - \frac{1}{4}(mR)^2 \right) \right)^{\frac{1}{2}} \end{aligned} \quad (\text{II.11})$$

Note that $k_R^2 < 0$ in this case, i.e., for $e_R^2 \tilde{\alpha} < \frac{1}{4}(mR)^2$.

Throughout, we will use the block notation to refer to the fermionic retarded (Feynman) propagators

$$\mathcal{G}_{R,F} = \begin{pmatrix} \mathcal{G}^{11} & \mathcal{G}^{12} \\ \mathcal{G}^{21} & \mathcal{G}^{22} \end{pmatrix}_{R,F} \quad (\text{II.12})$$

Case-2: $e_R^2 \tilde{\alpha} > \frac{1}{4}(mR)^2$

For $k_R^2 > 0$ and $k \leq k_R$, the corresponding holographic spectral function exhibits oscillating behavior and gapless excitations, with comparable real and imaginary parts. In other words, the excitations in this oscillating region are short lived as they form and quickly fall into the extremal RN-AdS black hole.

Further arguments [16, 17] show that the fermionic density diverges near the horizon causing strong back reaction. As a result, the near horizon geometry becomes a Lifshitz geometry whereby the Fermi-like volume is resolved into concentric Fermi spheres each describing heavy Fermions with narrow widths, thereby explaining the gapless like excitations. This resolution occurs only for $|k^0|/\mu \sim e^{-N_c^2}$ and resorbs for $|k^0|/\mu \sim N_c^0$.

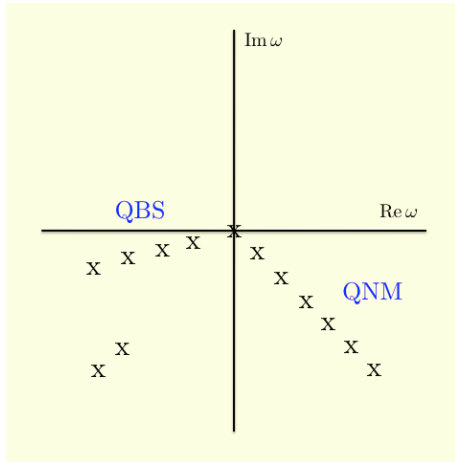


FIG. 2: Schematic description of the poles of the Green function. For sufficiently large U(1) charge e_R some of the quasi-normal modes (QNM) of the RN-AdS black-hole transmute to narrow quasi-bound states (QBS) by moving closer to the real-axis.

Case-3: $e_R^2 \tilde{\alpha} > \frac{1}{4}(mR)^2$

For $k_R^2 > 0$ and $k \geq k_R$, localized and long lived fermionic states emerge that are characterized by a Fermi momentum $k_F > k_R$. In this case, the retarded propagator near the Fermi surface reads [16, 17]

$$\mathcal{G}_R^{11}(k^0, \vec{k}) \approx \frac{h_1}{k - k_F - \frac{1}{v_F} k^0 - \Pi(k^0)} \begin{pmatrix} 0 & 0 \\ 0 & 1 \end{pmatrix} \quad (\text{II.13})$$

$$\text{Im } \mathcal{G}_R^{11}(\omega_1, k + q) \text{Im } \mathcal{G}_R^{11}(k^0, \vec{k}) \rightarrow \text{Tr} \left((\sigma_1(k^0 + q^0) - i\sigma_2(k_x + q_x) - \omega_1) \pi \delta((k + q)^2 + \omega_1^2) \text{Im } \mathcal{G}_R^{11}(k^0, \vec{k}) \right) \quad (\text{II.15})$$

III. HOLOGRAPHIC STRUCTURE FUNCTIONS

The holographic structure functions on an extremal black-hole in leading order have been discussed in [18], to which we refer for further details. For completeness, the results will be summarized below, and extended to allow for the next to leading order contributions from the

with

$$\begin{aligned} \Pi(k^0) &= h_2 e^{i\gamma k_F} (k^0)^{2\nu_k} \\ \nu_k &= \frac{\sqrt{\tilde{\alpha}}}{\mu} (k^2 - k_R^2)^{\frac{1}{2}} \\ \gamma_k &= \arg \left(\Gamma(-2\nu_k) \left(e^{-2\pi i \nu_k} - e^{-\frac{2\pi}{\sqrt{3}} e_R \sqrt{\tilde{\alpha}}} \right) \right). \end{aligned} \quad (\text{II.14})$$

The coefficients $h_1 \sim \frac{r_-}{R^2}$ and $h_2 \sim \left(\frac{r_-}{R^2} \right)^{1-2\nu_{k_F}}$ can be computed numerically. For $\nu_k > \frac{1}{2}$, $\nu_k = \frac{1}{2}$ or $\nu_k < \frac{1}{2}$ we have a Fermi liquid, a marginal Fermi liquid or a non-Fermi liquid, respectively. Note that the transition from a non-Fermi liquid to a Fermi liquid occurs for $k^0 \approx k_c^0$ which is fixed by the condition $k_c^0 \approx |v_F \Pi(k_c^0)|$. Below, we will refer to the non-Fermi liquid region $k^0 < k_c^0$ as the near horizon or emergent contribution, and the Fermi liquid region $k^0 > k_c^0$ as the far horizon or dilute contribution. The two contributions will be added approximately since an exact construction that interpolates between these two limiting regimes is likely numerical and outside the scope of this work.

A schematic description of the poles of (II.13) is given in Fig. 2. For sufficiently large effective charge $e_R \sqrt{\tilde{\alpha}}$, some of the largely damped quasi-normal modes (QNM) of the RN-AdS black hole transmute to narrow quasi-bound states (QBS) close to the real axis for fixed $k < k_F$. For increasing $k \rightarrow k_F$ the narrow QBS start crossing the origin $\omega = 0$ turning to equally spaced holographic Fermi surfaces (here 4 Fermi surfaces) as discussed in [17].

For fermions with larger effective charge, i.e., for $e_R^2 \tilde{\alpha} > \frac{1}{4}(mR)^2$ or $k_R^2 > 0$, pair creation takes place near the horizon as we noted earlier. A hallow of charged fermions at the Fermi surface with $k_F > k_R > 0$, that supports quasi-particles with \mathcal{G}_F^{11} given in (II.13). For hard R-probes with large q^0 in the DIS kinematics, only $\mathcal{G}_R^{11}(k^0, \vec{k})$ is modified close to the horizon, since $\mathcal{G}_R^{11}(\omega_1, k + q)$ carries a large momentum and is mostly unmodified in the ultraviolet,

holographic Fermi liquid at the horizon.

A. Structure functions

We recall that the scattering amplitude of an R-photon of longitudinal momentum $q^\mu = (\omega, q, 0, 0)$ scattering on a black-hole at rest in the Lab frame with $n^\mu = (1, 0, 0, 0)$,

(III.37), can be tensorially decomposed into two invariant functions $\tilde{G}_{1,2}$ [13]

$$\tilde{G}_{\mu\nu}^F(q) = \left(\eta_{\mu\nu} - \frac{q_\mu q_\nu}{Q^2} \right) \tilde{G}_1 + \left[n_\mu n_\nu - \frac{n \cdot q}{Q^2} (n_\mu q_\nu + n_\nu q_\mu) + \frac{q_\mu q_\nu}{(Q^2)^2} (n \cdot q)^2 \right] \tilde{G}_2 \quad (\text{III.16})$$

with $Q^2 = q^2$, thanks to with the current conservation and covariance. The corresponding DIS structure functions for an R-photon on a black hole are defined as

$$\begin{aligned} \tilde{F}_1 &= \frac{1}{2\pi} \text{Im} \tilde{G}_1, \\ \tilde{F}_2 &= -\frac{(n \cdot q)}{E_A} \text{Im} \frac{1}{2\pi} \tilde{G}_2. \end{aligned} \quad (\text{III.17})$$

As in [13], the rest frame of a cold and extremal black hole will be dual to the rest frame of a cold nucleus at the boundary with fixed energy $E_A = \frac{3}{4} A \mu$. Since the binding energy in a nucleus is small, we also have $E_A \simeq A m_N$ and therefore the chemical potential $\mu \simeq \frac{4}{3} m_N$. In our mapping, m_N and μ are interchangeable for estimates. A hard photon with virtual momentum $q^\mu = (\omega, q, 0, 0)$ scattering off the nucleus in the DIS kinematics satisfies $q^2 - \omega^2 \equiv Q^2 \rightarrow \infty$ with $\omega \simeq q$ and fixed Bjorken-x

$$x_A = \frac{q^2}{-2q \cdot (n E_A)} \equiv \frac{Q^2}{2E_A \omega} = \frac{x m_N}{E_A} \quad (\text{III.18})$$

B. Classical black-hole in leading order: small-x

As we noted earlier, the leading order contribution to the structure functions (III.17) in DIS scattering is classical and of order N_c^2 as illustrated in Fig. 1. It does not involve scattering off the fermions near the holographic surface, which is of order N_c^0 . In the regime $Q \ll q \ll Q^2/\mu$ the leading contribution to the structure functions vanishes, as the probe spin-1 R-field is prevented from falling to the black-hole by an induced potential barrier [12]. The R-current correlator is purely real with an exponentially vanishing imaginary part. In the regime $q \gg Q^3/\mu^2$, the barrier wanes away with the classical and leading contribution to the un-normalized structure function F_2 of the form [13]

$$\begin{aligned} \tilde{F}_2(x_A, Q^2) &\approx \\ \tilde{C}_T \frac{\mu^2}{x_A} \left(\frac{x_A^2 Q^2}{\mu E_A} \right)^{\frac{2}{3}} &+ \tilde{C}_L \frac{E_A}{\mu} \frac{\mu^2}{x_A} \left(\frac{x_A^2 Q^2}{\mu E_A} \right) \end{aligned} \quad (\text{III.19})$$

with

$$\begin{aligned} \tilde{C}_T &= \frac{N_c^2}{2^{17/3} \pi^2 \Gamma^2(1/3) \tilde{\alpha}^{5/3}} \\ \tilde{C}_L &= \frac{N_c^2}{1152 \pi^4 \tilde{\alpha}^2} \end{aligned} \quad (\text{III.20})$$

with $x_A E_A = x m_N$ and $C_L \ll C_T$. This result was shown to hold for low-x or $x_A \ll \sqrt{\mu E_A}/Q$, with the Callan-Gross relation-like $\tilde{F}_2 = 2x_A \tilde{F}_1$. The normalized structure functions follow as [13]

$$F_{1,2} \equiv 2E_A V_A \tilde{F}_{1,2} \equiv \left(\frac{12\pi \tilde{\alpha} A}{N_c \mu} \right)^2 \tilde{F}_{1,2} \quad (\text{III.21})$$

after using the black-hole equation of state. More specifically, we have ($Q^2 = q^2 > 0$)

$$\frac{F_2^{\text{BH}}(x, q^2)}{A} \approx \frac{C_T}{x} \left(\frac{3x^2 q^2}{4m_N^2} \right)^{\frac{2}{3}} + \frac{3C_L}{4x} \left(\frac{3x^2 q^2}{4m_N^2} \right) \quad (\text{III.22})$$

with $C_{T,L}/\tilde{C}_{T,L} = \pi^5 (48\tilde{\alpha})^2 / 2N_c^2$.

The normalization in (III.21) amounts overall to normalizing $\tilde{F}_{1,2}$ by the density of the black-hole, canceling part of the model dependence of the equation of state. In a way, the normalized $F_{1,2}$ are the un-normalized black-hole structure functions $\tilde{F}_{1,2}$ per degree of freedom. (III.22) is dominated by the first contribution at low-x. We now show that the next contribution is dominated by scattering off bulk fermions at large-x from a holographic Fermi liquid close to the horizon.

C. Classical black-hole in leading order: large-x

The large-x contribution to the dense black-hole can be obtained using the WKB approach also developed for the thermal black hole in [12] with similar results modulo pertinent changes in the parameters and normalization. In particular, the structure function for $x > \mu/q$ is found to drop exponentially with the result

$$\frac{F_2^{\text{BH}}(x, q^2)}{A} \approx \frac{3C_L}{2x} \left(\frac{3x^2 q^2}{4m_N^2} \right) D(x), \quad (\text{III.23})$$

where to exponential accuracy

$$D(x) \approx C_D e^{-\sqrt{\frac{q}{m_N} \frac{m_N}{\mu}} \sqrt{x}}, \quad (\text{III.24})$$

with $C_D \approx e^{-\frac{2\Gamma^2(1/4)\sqrt{6\alpha}}{3\sqrt{2\pi}}}$. Below we will use (III.22) plus (III.23) to describe DIS scattering on the BH in leading order. We now proceed to analyze the quantum and sub-leading correction.

D. Quantum fermions in sub-leading order

The contribution of the sub-leading fermions to the induced effective action can be obtained through the holographic dictionary. It will be divided into two contributions: 1/ the one stemming from the emergent Fermi

surface near the horizon through the geometrical reduction to $\text{AdS}_2 \times \mathbb{R}^3$; 2/ the one stemming from its ultraviolet completion which is dual to a Fermi liquid in bulk AdS_5 which we will seek in the dilute approximation below.

With this in mind, the shift of the R-field $A_M \rightarrow A_0 \delta_{M0} + a_M$ amounts to a shift in the Dirac action density in (II.8) at the origin of the minimal coupling of the R-field

$$-i\bar{\psi}(-ie_R a_\mu(r, q)\Gamma^\mu)\psi \equiv \bar{\psi}B(r; q)\psi \quad (\text{III.25})$$

In terms of (II.8-III.25) the bulk effective action for the 1-loop contribution in Fig. 1b at *zero temperature* reads

$$\mathcal{S}_F[a_\mu] = -(-i) \int \frac{d^4 q}{(2\pi)^4} \frac{d^4 k}{(2\pi)^4} \int dr_1 \sqrt{g(r_1)} dr_2 \sqrt{g(r_2)} \text{Tr} \left(D_F(r_1, r_2; k+q) B(r_2; q) D_F(r_2, r_1; k) B(r_1; q) \right) \quad (\text{III.26})$$

The routing of the momenta in (III.26) corresponds to the hard fermion with $k+q$ and the soft fermion with k .

The R-field in bulk $a(r, q)$ relates to the R-field at the boundary $A_\mu^{(0)}(q)$ through the bulk-to-boundary propagator $K_A(r; q)$, which satisfies $K_A(r \rightarrow \infty; q) = 1$,

$$a_\mu(r; q) = K_A(r; q) A_\mu^{(0)}(q). \quad (\text{III.27})$$

This allows the re-writing of (III.26) in the form of the boundary action

$$\begin{aligned} \mathcal{S}_F[A_\mu^{(0)}] &= \frac{1}{2} \int \frac{d^4 q}{(2\pi)^4} A_\mu^{(0)}(q) A_\nu^{(0)}(-q) \\ &\times (-2i) \int \frac{d^4 k}{(2\pi)^4} \int dr_1 dr_2 \sqrt{g(r_1)} \sqrt{g(r_2)} \text{Tr} \left(D_F(r_1, r_2; k+q) Q^\mu(r_2; q) D_F(r_2, r_1; k) Q^\nu(r_1; q) \right) \end{aligned} \quad (\text{III.28})$$

with the dressed bulk vertices

$$\begin{aligned} Q^\mu(r; q) &= -i \left(-ie_R K_A(r; q) \Gamma^\mu \right) \\ &\approx -e_R \frac{qR^2}{r} K_1 \left(\frac{qR^2}{r} \right) \Gamma^\mu. \end{aligned} \quad (\text{III.29})$$

We have approximated the bulk-to-boundary $K_A(r; q)$ by its vacuum contribution, with $K_1(x)$ the modified Bessel function.

In the DIS regime $Q \ll q \ll Q^2/\mu$ with $Q^2 = q^2$, the spin- $\frac{1}{2}$ fermion field remains localized near the boundary

as a potential barrier develops in bulk, a phenomenon also observed for spin-1 boson fields [12]. In this regime, we will approximate the hard part of the fermion propagator by its vacuum (in AdS_5) result [20]

$$D_F(r_1, r_2; k+q) = \int d\omega_1 \omega_1 G_F(r_1, r_2; \omega_1, k+q), \quad (\text{III.30})$$

where

$$G_F(r, r'; \omega_1, k + q) = \psi_\alpha(r, \omega_1) \mathcal{G}_F^{\alpha\gamma}(\omega_1, k + q) \overline{\psi}_\gamma(r', \omega_1) \quad (\text{III.31})$$

with the vacuum (in AdS₅) solution [21]

$$\begin{aligned} \psi_1(r, \omega_1) &= \left(\frac{R^2}{r}\right)^{\frac{5}{2}} J_{mR-\frac{1}{2}}\left(\omega_1 \frac{R^2}{r}\right) \begin{pmatrix} 0 \\ 1 \end{pmatrix} \\ \psi_2(r, \omega_1) &\equiv 0, \end{aligned} \quad (\text{III.32})$$

and

$$\begin{aligned} \mathcal{G}_F^{11}(\omega_1, k + q) &= \frac{\sigma_1(k^0 + q^0) - i\sigma_2(k_x + q_x) - \omega_1}{(k + q)^2 + \omega_1^2 - i\epsilon}, \\ \mathcal{G}_F^{22}(\omega_1, k + q) &= \frac{\sigma_1(k^0 + q^0) + i\sigma_2(k_x + q_x) - \omega_1}{(k + q)^2 + \omega_1^2 - i\epsilon}. \end{aligned} \quad (\text{III.33})$$

The soft part of the fermion propagator can be separated into its contribution deep in the infrared which is modified by the induced holographic Fermi surface through the geometrical reduction to AdS₂×R³, and its ultraviolet completion as we noted earlier. More specifically, near the AdS₂×R³ geometry, the infrared part of the soft the propagator is of the form

$$D_F(r, r'; k) = \psi_\alpha(r, k^0, \vec{k}) \mathcal{G}_{\alpha\beta}^F(k^0, \vec{k}) \overline{\psi}_\beta(r', k^0, \vec{k}) \quad (\text{III.34})$$

with

$$\begin{aligned} \mathcal{G}_F^{22}(k^0, \vec{k}) &= \\ \mathcal{G}_F^{11}(k^0, \vec{k} \mapsto -\vec{k}) &= -\frac{1}{\mathcal{G}_F^{11}(k^0, \vec{k}; m \mapsto -m)}. \end{aligned} \quad (\text{III.35})$$

Note that only $\mathcal{G}_R^{11}(k^0, \vec{k})$ has a singular or Fermi-like structure near $k \rightarrow k_F$. Hence, we will ignore the contribution from $\mathcal{G}_R^{22}(k^0, \vec{k})$ to the current correlator. The normalizable wave functions are given in (B.1).

The time-ordered correlation function for the R-current follows from the functional derivative

$$\tilde{G}^{F\mu\nu}(q) = \frac{\delta^2 \mathcal{S}_F[A_\mu^{(0)}]}{\delta A_\mu^{(0)}(q) \delta A_\nu^{(0)}(-q)}, \quad (\text{III.36})$$

Using the spectral form of the Feynman propagator (III.34-III.35), we can re-write (III.36) in a more compact form

$$\tilde{G}^{F\mu\nu}(q) = 2i \int \frac{d^4 k}{(2\pi)^4} \int d\omega_1 \omega_1 \text{Tr} \left(\mathcal{G}_F^{\alpha\beta}(\omega_1, k + q) \Lambda_{\beta\gamma}^\mu(\omega_1; q; k) \mathcal{G}_F^{\gamma\delta}(k^0, \vec{k}) \Lambda_{\delta\alpha}^\nu(k; q; \omega_1) \right), \quad (\text{III.37})$$

with the dressed vertices

$$\begin{aligned} \Lambda_{\beta\gamma}^\mu(\omega_1; q; k) &= \\ \int dr_2 \sqrt{g(r_2)} \overline{\psi}_\beta(r_2, \omega_1) Q^\mu(r_2; q) \psi_\gamma(r_2, k), \end{aligned} \quad (\text{III.38})$$

and

$$\begin{aligned} \Lambda_{\delta\alpha}^\nu(k; q; \omega_1) &= \\ \int dr_1 \sqrt{g(r_1)} \overline{\psi}_\beta(r_1, k) Q^\nu(r_1; q) \psi_\alpha(r_1, \omega_1). \end{aligned} \quad (\text{III.39})$$

We recall that at zero temperature, the general Feynman and retarded propagators $\mathcal{G}_{F,R}$ are related by the relationship

$$\mathcal{G}_F(k^0, \vec{k}) = \text{Re} \mathcal{G}_R(k^0, \vec{k}) + i \text{sgn}(k^0) \text{Im} \mathcal{G}_R(k^0, \vec{k}) \quad (\text{III.40})$$

Using (III.40) and the fact that $\mathcal{G}_F(k^0, \vec{k})$ is analytic in the upper complex k^0 -plane, allow for the re-writing of the imaginary part of (III.37) in the form

$$\begin{aligned}
\text{Im } \tilde{G}_{\mu\nu}^F(q) &= \int \frac{d^4 k}{(2\pi)^4} \int d\omega_1 \omega_1 \Lambda_{\beta\gamma}^\mu(\omega_1; q; k) \Lambda_{\delta\alpha}^\nu(k; q; \omega_1) \text{Re Tr} \left(\mathcal{G}_F^{\alpha\beta}(\omega_1, k+q) \mathcal{G}_F^{\gamma\delta}(k^0, \vec{k}) \right), \\
&= \int \frac{d^3 k}{(2\pi)^3} \int_{-|q^0|}^0 \frac{dk^0}{2\pi} \int d\omega_1 \omega_1 \Lambda_{\beta\gamma}^\mu(\omega_1; q; k) \Lambda_{\delta\alpha}^\nu(k; q; \omega_1) \text{Tr} \left(\text{Im } \mathcal{G}_R^{\alpha\beta}(\omega_1, k+q) \text{Im } \mathcal{G}_R^{\gamma\delta}(k^0, \vec{k}) \right),
\end{aligned} \tag{III.41}$$

This result shows that for $q^0 = 0$, the imaginary part vanishes as it should as the effective action induced by the R-current (III.28) is real. For $q^0 \neq 0$ this result is clearly negative as it should, since its contribution to (III.28) amounts to a self-energy for the R-field which amounts to damped oscillations in time.

E. Large- x near the horizon

Using the vertex (D.5) for momenta near k_F , we can re-write (III.41)

$$\begin{aligned}
\text{Im } \tilde{G}_{xx}^F(q) &= C^2(\nu_{k_F}) C_\theta k_F^2 \\
&\times (-1) \int_0^\infty \frac{d\omega_1^2}{2} I_z^2(\omega_1; q; k_F) \int_{k_R}^{k_F} dk a_+(k_0, k)^2 \text{Re } I_{k^0}(\omega_1, q),
\end{aligned} \tag{III.42}$$

with

$$\begin{aligned}
\text{Re } I_{k^0}(\omega_1, q) &= \text{Re} \int_{-\infty}^\infty \frac{dk^0}{2\pi} a_+(k_0, k)^2 \text{tr} \left(\mathcal{G}_F^{11}(\omega_1, k+q) \mathcal{G}_F^{11}(k^0, \vec{k}) \right) \\
&= \text{Re} \int_{-|q^0|}^0 \frac{dk^0}{2\pi} a_+(k_0, k)^2 \text{tr} \left((\sigma_1(k^0 + q^0) - i\sigma_2(k_x + q_x) - \omega_1)\pi \delta((k+q)^2 + \omega_1^2) \text{Im } \mathcal{G}_R^{11}(k^0, \vec{k}) \right) \\
&\approx \int_{-|q^0|}^0 \frac{dk^0}{2\pi} a_+(k_0, k)^2 (-1)\omega_1\pi \delta((k+q)^2 + \omega_1^2) \frac{h_1 \text{Im } \Pi}{(k - k_F - \frac{k^0}{v_F} - \text{Re } \Pi)^2 + (\text{Im } \Pi)^2}
\end{aligned} \tag{III.43}$$

(III.43) can be simplified by enforcing the delta function

$$\begin{aligned}
\text{Im } \tilde{G}_{xx}^F(q) &\approx C^2(\nu_{k_F}) C_\theta k_F^2 \frac{\pi}{2} \int_{k_R}^{k_F} dk \int_{-|q^0|}^0 \frac{dk^0}{2\pi} a_+^2(k_0, k) I_z^2(x_k; q; k_F) \sqrt{s_k} \frac{h_1 \text{Im } \Pi}{(k - k_F - \frac{k^0}{v_F} - \text{Re } \Pi)^2 + (\text{Im } \Pi)^2} \\
&\approx C_G(\nu_{k_F}, z_-) \left(\frac{1}{q^2} \right)^{\nu_{k_F} + \frac{3}{2}} \int_{k_R}^{k_F} dk k_F^2 \int_{-|q^0|}^0 \frac{dk^0}{2\pi} \\
&\times a_+^2(k_0, k) x_k^{\nu_{k_F} + 5/2} (1 - x_k)^{mR - 1/2} {}_2F_1^2 \left(\frac{mR + \nu_{k_F} + 2}{2}, \frac{mR - \nu_{k_F} + 1}{2}, mR + \frac{1}{2}, 1 - x_k \right) \\
&\times \sqrt{s_k} \frac{\text{Im } \Pi}{(k - k_F - \frac{k^0}{v_F} - \text{Re } \Pi)^2 + (\text{Im } \Pi)^2}
\end{aligned} \tag{III.44}$$

with the overall constant

$$C_G(\nu_{k_F}, z_-) = \frac{\pi}{2} z_-^{-(2\nu_{k_F} + 2)} C^2(\nu_{k_F}) C_z^2(\nu_{k_F}) \tilde{h}_1(\nu_{k_F}) C_\theta, \tag{III.45}$$

where $\tilde{h}_1(\nu_{k_F}) \equiv z_- h_1$ is a dimensionless constant to be determined numerically, and $z_- = \frac{R^2}{r_-}$. Again, for the DIS kinematics we set $x_k = -q^2/2k \cdot q$, and $|q^0| \approx q_x$. We re-arranged the hypergeometric function ${}_2F_1$ using the same Pfaff identity (III.51). Note that for the special value of $\nu_k = mR+1$, one can see that the x_k dependence of the integrand in (III.44) reduces to the one in [21] before the multiplication by the trace (for our case the trace is $\sqrt{s_k}$). However, for general ν_k the same partonic content as in (III.52) is noted.

For narrow quasi-particles, we may use the substitution ($k_\perp = k - k_F$)

$$\frac{\text{Im } \Pi}{(k_\perp - \frac{k^0}{v_F} - \text{Re } \Pi)^2 + (\text{Im } \Pi)^2} \rightarrow \pi \delta \left(k_\perp - \frac{k^0}{v_F} - \text{Re } \Pi \right) \quad (\text{III.46})$$

and undo the k^0 integration in (III.44) with the result

$$\text{Im } \tilde{G}_{xx}^F(q) \approx \frac{1}{2} \tilde{C}_G(\nu_{k_F}) \int_{k_R}^{k_F} dk_\perp k_F^2 \frac{a_+(k_0, k_\perp)^2}{\left| \frac{1}{v_F} + \text{Re } \Pi' \right|} \left(\frac{1}{q^2 z_-^2} \right)^{\nu_{k_F}+1} x_k^{\nu_{k_F}+2} (1-x_k)^{\tau-\frac{3}{2}} {}_2F_1^2(\tau_+, \tau_-, \tau-1, 1-x_k) \quad (\text{III.47})$$

with

$$\text{Re } \Pi' = 2h_2 \nu_{k_F} |k^0|^{2\nu_{k_F}-1} \text{Re} \left(e^{i\gamma_{k_F}} (-1)^{2\nu_{k_F}-1} \right) \quad (\text{III.48})$$

where k^0 in x_k is solution to the transcendental equation

$$k_\perp + \frac{|k^0|}{v_F} = h_2 |k^0|^{2\nu_{k_F}} \text{Re} \left(e^{i\gamma_{k_F}} (-1)^{2\nu_{k_F}} \right), \quad (\text{III.49})$$

and we have defined a dimensionless constant

$$\begin{aligned} \tilde{C}_G(\nu_{k_F}) &= z_-^{2\nu_{k_F}+2} \times C_G(\nu_{k_F}, z_-) \\ &= \frac{\pi}{2} C^2(\nu_{k_F}) C_z^2(\nu_{k_F}) \tilde{h}_1(\nu_{k_F}) C_\theta. \end{aligned} \quad (\text{III.50})$$

Also note that $a_+(k_0, k_\perp) = \bar{c}_1 z_- k_\perp + \bar{c}_2 z_- k_0$ is a dimensionless coefficient with dimensionless constants $\bar{c}_{1,2} = \tilde{c}_{1,2}/z_-$.

In arriving to (III.47), we have made use of the Pfaff identity

$${}_2F_1(a, b, c, z) = (1-z)^{-a} {}_2F_1\left(a, c-b, c, \frac{z}{z-1}\right) \quad (\text{III.51})$$

In the holographic Fermi liquid, the partonic distribution function is seen to develop a modified exponent. A comparison of the partonic distribution function (VI.96) in the probe limit, to (F.4) where the black hole is present, translates

$$\left(\frac{1}{q^2} \right)^{\tau-1} x_k^{\tau+1} (1-x_k)^{\tau-2} \rightarrow \left(\frac{1}{q^2} \right)^{\nu_k+1} x_k^{\nu_k+2} (1-x_k)^{\tau-\frac{3}{2}} {}_2F_1^2(\tau_+, \tau_-, \tau-1, 1-x_k) \quad (\text{III.52})$$

with $2\tau_\pm = \tau \pm (\nu_k + 1/2)$ and the twist parameter $\tau = mR + 3/2$. Near the black hole horizon, the parton distribution function develops a modified scaling law, but it is still seen to vanish at the end points $x_k = 0, 1$. In Fig. 3 we show the modified behavior of the partonic distribution function in (III.52) for fixed q^2 , $\tau = 3$ and $\nu_k = \frac{1}{2}$ versus x_k as the light-solid curve (green). The comparison is with the large- x dependence of the nucleon for weak coupling dashed curve (red), and strong cou-

pling dark-solid curve (blue). Near the black hole horizon, the distribution function is shifted to intermediate- x . With our choice of parameters, the holographic result (III.52) reduces to $x_k^{\frac{1}{2}}(1-x_k)^{\frac{3}{2}}$, in comparison to the strong coupling result in vacuum $x_k^4(1-x_k)^2$, and the weak coupling result also in the vacuum $x_k^{\frac{1}{2}}(1-x_k)^3$. Remarkably, the formation of a holographic fermionic surface through the $\text{AdS}_2 \times \text{R}^3$ reduction, is to shift the

holographic partonic distribution to intermediate-x, and modify the hard scattering rule.

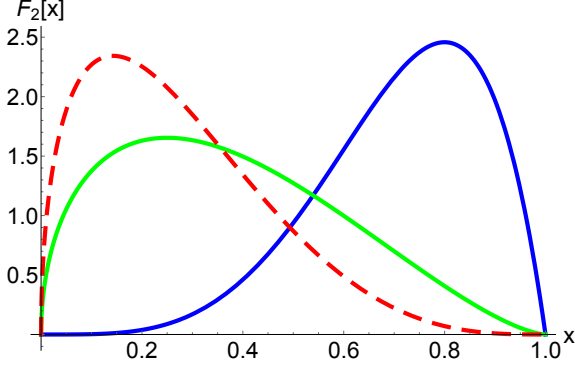


FIG. 3: Large-x dependence of the parton distribution function for weak coupling in vacuum (dashed-red), strong coupling in vacuum (dark-solid-blue) and near a holographic Fermi surface (light-solid-green).

For our choice of DIS kinematics, the non-normalized \tilde{F}_2 structure function (III.17) follows from (III.47) in the form ($q_0 \approx q_x$)

$$\tilde{F}_2(x_A, q) = \frac{4}{\pi} x_A^3 \frac{E_A^2}{q^2} \text{Im} \tilde{G}_{xx}^F(q) \quad (\text{III.53})$$

$$\begin{aligned} \mathcal{S} &= \int d^{10}x \sqrt{-g_{10}} (\mathcal{KV})_{t=0} \\ &= \frac{i}{8} \int d^{10}x \sqrt{-g_{10}} (4v^a v_a \bar{\psi} \Gamma_m \partial^p \psi - g_m^p (\bar{\psi} \Gamma^M \partial_M \psi v_a v^a + 2v_a v_b \bar{\psi} \Gamma^a \partial^b \psi)) F^{mn} F_{pn} \mathcal{V}|_{t=0} \end{aligned} \quad (\text{IV.54})$$

where v^a are the Killing vectors for the compact part of the 10-dimensional space. The forward R-current scattering amplitude follows from pertinent variation with respect to the R-field. Here \mathcal{K} refers to the kinematical factor involving the fermions ψ and the R-field strength F , and \mathcal{V} is the exchanged flat space 10-dimensional Virazoro-Shapiro string amplitude

$$\mathcal{V} = \frac{\alpha'^3 \tilde{s}^2}{64} \prod_{\tilde{\beta}=\tilde{s}, \tilde{t}, \tilde{u}} \frac{\Gamma\left(-\frac{\alpha' \tilde{\beta}}{4}\right)}{\Gamma\left(1 + \frac{\alpha' \tilde{\beta}}{4}\right)} \quad (\text{IV.55})$$

as illustrated in Fig. 4. The 10-dimensional Mandelstam variables \tilde{s}, \tilde{t} are related to the 4-dimensional ones s, t through

with again $Q^2 = q^2 > 0$. Modulo the dispersion relation and the anomalous exponents that characterize the holographic fermions in the reduced $\text{AdS}_2 \times \text{R}^3$ geometry, the results (III.47) and (III.53) are similar to the ones we derived recently in [18] using general arguments.

IV. FERMIONIC CONTRIBUTION AT LOW-X

In the DIS regime with $q \gg Q^2$ or low-x, the structure functions are dominated by the exchange of a Pomeron, a multigluon exchange with vacuum quantum numbers. In holography, this exchange is described either through a closed surface exchange [23] or a graviton [24] in bulk. For the latter, this regime was identified in the range $e^{-\sqrt{\lambda}} \ll x \ll 1/\sqrt{\lambda}$ where the exchange involves the string scattering amplitude. Since $x \gg e^{-\sqrt{\lambda}}$, the strings are small compared to the size of the AdS space so that the scattering amplitude is quasi-local with almost flat space signature.

A. General set up

The 10-dimensional tree-level effective action that describes the scattering of an R-photon off bulk quantum fermions at low-x reads [24]

$$\begin{aligned} \alpha' \tilde{s} &= \alpha' s \frac{z^2}{R^2} + \mathcal{O}\left(\frac{1}{\sqrt{\lambda}}\right) \\ \alpha' \tilde{t} &= \alpha' t \frac{z^2}{R^2} + \mathcal{O}\left(\frac{1}{\sqrt{\lambda}}\right) \end{aligned} \quad (\text{IV.56})$$

with the warping made explicit.

The imaginary part of the string amplitude (IV.55) is

$$\text{Im} \mathcal{V}|_{t=0} = \frac{\pi \alpha'}{4} \sum_{j=1}^{\infty} j^{\mathcal{O}\left(\frac{1}{\sqrt{\lambda}}\right)} \delta\left(j - \frac{\alpha' \tilde{s}}{4}\right) \quad (\text{IV.57})$$

with the delta-function summing over the closed string Regge trajectory. At low-x we have $s \sim 1/x$ and $j \sim s \sim$

$1/x$, so that for $\ln(1/x)/\sqrt{\lambda} \ll 1$,

$$j^{\mathcal{O}}\left(\frac{1}{\sqrt{\lambda}}\right) \sim \left(\frac{1}{x}\right)^{\mathcal{O}\left(\frac{1}{\sqrt{\lambda}}\right)} \sim 1 \quad (\text{IV.58})$$

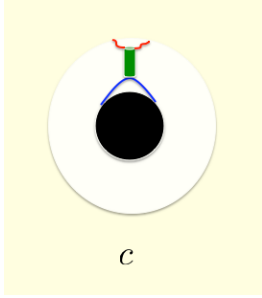


FIG. 4: Absorptive part of the R-current on a nucleus as an extremal RN-AdS black hole: (c) fermionic contribution to order N_c^0 due to a closed string exchange in bulk at low-x.

We now recall that the field strength F^{mn} describes the bulk-to-boundary R-field-strength with incoming momentum q^μ and outgoing momentum q^μ , while ψ describes the bulk fermion with incoming and outgoing momentum k^μ in the anomalous Fermi surface. The low-x regime with $x \ll 1$ corresponds to the kinematical regime $q \cdot k \gg q^2 \gg k^2$, so that the dominant contribution in \mathcal{K} is the term with the spin contraction of the form $(q \cdot k)$, i.e. the first term in (IV.54). Using

$$\psi(k) \rightarrow \psi(k) \times \mathbb{Y}(v) \quad (\text{IV.59})$$

and normalizing

$$\int_{S^5} d\hat{v} \sqrt{g_{S^5}} v^a v_a |\mathbb{Y}(v)|^2 = c_5 R^2 \quad (\text{IV.60})$$

where $\mathbb{Y}(v)$ is a spherical harmonic in S^5 in (IV.54), we can write down the one-loop effective action \mathcal{S}_F for the diagram shown in Fig. 4 as

$$\mathcal{S}_F[A_\mu^{(0)} \equiv n_\mu] = \frac{i}{2} c_5 R^2 \int \frac{d^4 q}{(2\pi)^4} \int \frac{d^4 k}{(2\pi)^4} \int dr \sqrt{-g} F^{\mu m}(-q) F_{\nu m}(q) \text{Tr} (D_F(r, r, k) \Gamma_\mu(-ik)^\nu) \mathcal{V}_F|_{t=0} \quad (\text{IV.61})$$

We now choose the polarizations to be transverse with the additional axial gauge condition $a_r = 0$, so that the boundary-to-bulk R-field is

$$a_\mu(r, \vec{q}) = \left(\frac{R^2}{r} K_1 \left(\frac{qR^2}{r} \right) \right) n_\mu(q) e^{iq \cdot x} \quad (\text{IV.62})$$

The corresponding field strengths are

$$\begin{aligned} F_{\mu\nu}(q) &= i(q_\mu n_\nu - n_\mu q_\nu) \frac{qR^2}{r} K_1 \left(\frac{qR^2}{r} \right) e^{iq \cdot x}, \\ F_{\mu r}(q) &= n_\mu q^2 \frac{R^4}{r^3} K_0 \left(\frac{qR^2}{r} \right) e^{iq \cdot x} \end{aligned} \quad (\text{IV.63})$$

and their contraction is

$$\begin{aligned} F_{\mu p} F_\nu{}^p &= +n_\mu n_\nu \frac{q^4 R^6}{r^4} \left(K_0^2 \left(\frac{qR^2}{r} \right) + K_1^2 \left(\frac{qR^2}{r} \right) \right) \\ &+ q_\mu q_\nu n^2 \frac{q^2 R^6}{r^4} K_1^2 \left(\frac{qR^2}{r} \right) \end{aligned} \quad (\text{IV.64})$$

B. Low-x near the horizon

To analyze the low-x contribution of the fermions near the horizon, we will focus on the graviton exchange and make use of warped momenta \tilde{q} throughout this section. For small energy transfer $\tilde{q}_0 \ll \mu$, the bulk-to-bulk propagator for transverse graviton $h_x{}^y(\tilde{q}_0, \tilde{q}_x)$ can be written as

$$G_{xy,xy}(\tilde{q}_0, \tilde{q}_x, r_1, r_2) = \phi(\tilde{q}_0, \tilde{q}_x, r_1) G_{xy,xy}^B(\tilde{q}_0, \tilde{q}_x) \phi(q_0, q_x, r_2) \quad (\text{IV.65})$$

where $\phi(\tilde{q}_0, \tilde{q}_x, r_1)$ is the normalizable wave function of the graviton, and $G_{xy,xy}^B$ is its boundary Green's function

$$G_{xy,xy}^B(\tilde{q}_0, \tilde{q}_x) = \tilde{q}_0^2 G(\tilde{q}_0, \tilde{q}_x) \quad (\text{IV.66})$$

where $\text{Re } G(\tilde{q}_0, \tilde{q}_x) = f(\tilde{q}_x, \mu)$ which can be determined from the low-frequency expansion, and [27]

$$\begin{aligned} \text{Im } G(\tilde{q}_0, \tilde{q}_x) &= \frac{3C}{\left(1 + \frac{\tilde{q}_0^2}{\mu^2}\right)^{\frac{1}{2}}} \left(1 + \left(1 + \frac{\tilde{q}_0^2}{\mu^2}\right)^{\frac{1}{2}}\right) \\ &\times e_0 \left(\frac{\tilde{q}_x}{\mu}\right) \text{Im} \mathcal{G}_{\pm} \left(\frac{\tilde{q}_0}{\mu}, \frac{\tilde{q}_x}{\mu}\right) \end{aligned} \quad (\text{IV.67})$$

where C is a proportionality constant, $e_0\left(\frac{\tilde{q}_x}{\mu}\right)$ is a function to be determined from the low-frequency expansion coefficients, and

$$\mathcal{G}_{\pm} \left(\frac{\tilde{q}_0}{\mu}, \frac{\tilde{q}_x}{\mu}\right) = -2\nu_{\pm} e^{-i\pi\nu_{\pm}} \frac{\Gamma(1 - \nu_{\pm})}{1 + \nu_{\pm}} \left(\frac{1}{2} \frac{\tilde{q}_0}{\mu}\right)^{2\nu_{\pm}}, \quad (\text{IV.68})$$

where

$$\nu_{\pm} = \frac{1}{2} \left(5 + 2 \frac{\tilde{q}_x^2}{\mu^2} \pm 4 \left(1 + \frac{\tilde{q}_x^2}{\mu^2}\right)^{\frac{1}{2}}\right)^{\frac{1}{2}}. \quad (\text{IV.69})$$

Note that for zero energy and momentum transfer ($\tilde{q}_0 = 0$ and $\tilde{q}_x = 0$), the bulk-to-bulk propagator of the graviton exchange vanishes $\text{Im } G_{xy,xy}(0, 0, r_1, r_2) = 0$ since $\mathcal{G}_{\pm}(0, 0) = 0$. Therefore, the t-channel contribution of the graviton for the current-current correlation function or forward deeply virtual Compton scattering away from the probe limit vanishes. Its Reggeized form through higher spins (closed string exchange), vanishes as well.

V. R-RATIO FOR A QUANTUM CORRECTED RN-ADS BLACK-HOLE

A. Particle and energy density at the horizon

Having assessed the structure functions both at large- x and small- x near the black hole horizon, we now need to normalize them. For that we need to evaluate the contribution of the bulk fermions near the horizon to the particle and energy densities, much like we did in the probe limit. More specifically, we define

$$\begin{aligned} ne_R &= \langle J^t \rangle (qz \ll 1) \\ \epsilon &= \langle T^{tt} \rangle (qz \ll 1) \end{aligned} \quad (\text{V.70})$$

as the boundary expectation values of the time-component of the R-current and the energy momentum

tensor. The expectation values follow from the holographic correspondence in the tadpole approximation in AdS as

$$\begin{aligned} \langle J^t \rangle &= -ie_R \int \frac{d^3k}{(2\pi)^3} \int \frac{dk^0}{2\pi} I_K(qz \ll 1) \\ &\times \overline{\psi}_1(k) \Gamma^t \psi_1(k) \text{Im Tr } \mathcal{G}_R^{11}(k^0, \vec{k}) \\ \langle T^{tt} \rangle &= \int \frac{d^3k}{(2\pi)^3} \int \frac{dk^0}{2\pi} I'_K(qz \ll 1) \\ &\times \overline{\psi}_1(k) \Gamma^t \psi_1(k) (-ik^0) \text{Im Tr } \mathcal{G}_R^{11}(k^0, \vec{k}) \end{aligned} \quad (\text{V.71})$$

with $I'_K(qz \ll 1) \approx I_K(qz \ll 1)$ playing the role of a spectral weight, and defined in (VI.106). Evaluating the momentum integral near the Fermi surface, we find

$$n = \frac{\langle J^t \rangle}{e_R} \approx C_J h_1 C_{\theta} \frac{k_F^3 (1 - \frac{k_R}{k_F})}{\left[\frac{1}{v_F} + \text{Re } \Pi'\right]} \quad (\text{V.72})$$

with $C_{\theta} = \frac{1}{2\pi}$ and the dimensionless constant

$$\begin{aligned} C_J &= R^4 (mR_2 + \nu_{k_F}) \left(\frac{R_2}{R} k_F z_- + e_R \sqrt{\frac{\tilde{\alpha}}{3}}\right) \\ &\times \frac{a_{\pm}^2(k_0, k)}{(2\nu_k + 1)W^2} (2\sqrt{3})^{-2\nu_{k_F}} \end{aligned} \quad (\text{V.73})$$

Since $I_K = I'_K$, we have $\epsilon = nk^0$. Note that k_0 is the solution of the transcendental equation (III.49), which near the Fermi surface $k \rightarrow k_F$ can be solved as $k_0 \sim C_0/z_-$ with the dimensionless constants

$$C_0(\nu_{k_F}) \equiv (v_F \tilde{h}_2 \text{Im}(e^{i\gamma_F} (-1)^{2\nu_{k_F}}))^{-\frac{1}{1-2\nu_{k_F}}} \quad (\text{V.74})$$

and $\tilde{h}_2 = z_-^{1-2\nu_{k_F}} h_2$. Therefore, for the dense limit near the horizon, we make the identification $E_A \equiv V_A \epsilon = A \epsilon/n = A k^0$.

B. Normalized structure functions : dense regime

Having determined n, ϵ in the dense limit near the horizon, we can now normalize the corresponding structure function (III.47) through the substitution

$$\text{Im } \tilde{G}_{xx}^F(q) \rightarrow 2E_A V_A \times \text{Im } \tilde{G}_{xx}^F(q) = 2E_A A \frac{\text{Im } \tilde{G}_{xx}^F(q)}{n} \quad (\text{V.75})$$

The integral in (III.47) can be evaluated near the fermi surface $k \rightarrow k_F$ with the result

$$\text{Im } \tilde{G}_{xx}^F(q) \approx \frac{1}{2} \tilde{C}_G(\nu_{k_F}) a_+(k_0, k_\perp = 0)^2 \frac{k_F^3 \left(1 - \frac{k_R}{k_F}\right)}{\left|\frac{1}{v_F} + \text{Re } \Pi'\right|} \left(\frac{1}{q^2 z_-^2}\right)^{\nu_{k_F}+1} x_{k_F}^{\nu_{k_F}+2} (1 - x_{k_F})^{\tau - \frac{3}{2}} {}_2F_1^2(\tau_+, \tau_-, \tau - 1, 1 - x_{k_F}), \quad (\text{V.76})$$

Here $\tilde{C}_G(\nu_{k_F})$ and $a_+(k_0, k_\perp = 0) \approx \bar{c}_2 z_- k_0$ are both dimensionless constants, and $x_{k_F} \approx \frac{E_A}{k_0} x_A = \frac{m_N}{k_0} x$ since $\frac{x_A}{x} = \frac{m_N}{E_A}$. Here $k_0 \sim C_0/z_-$ plays the role of the Fermi energy of the quasi-particles in the holographic Fermi liquid near the horizon z_- . We recall that

$$\frac{1}{z_-} = \frac{r_-}{R^2} = \frac{1}{2\sqrt{3}} \frac{\mu}{\sqrt{\tilde{\alpha}}} = \frac{R_2}{R} \frac{\mu}{\sqrt{\tilde{\alpha}}}, \quad (\text{V.77})$$

with $\tilde{\alpha} = 1$ for a U(1) R-charge, and $\tilde{\alpha} = \frac{1}{4} \frac{N_c}{N_f}$ for a D3-D7 U(1) vector charge.

Using III.53) together with (V.75-V.76), we can extract the normalized structure function of the holographic Fermi liquid ($x_{k_F} k_0 = x m_N$)

$$\frac{F_2(x_A, q^2)}{A} = e_R^2 C_{AdS2}(e_R, \tau, \tilde{\alpha}, v_F, \tilde{h}_2) \left(\frac{\mu^2}{q^2}\right)^{\nu_{k_F}+2} x_{k_F}^{\nu_{k_F}+5} (1 - x_{k_F})^{\tau - \frac{3}{2}} {}_2F_1^2(\tau_+, \tau_-, \tau - 1, 1 - x_{k_F}), \quad (\text{V.78})$$

where we defined the dimensionless constant

$$C_{AdS2}(e_R, \tau, \tilde{\alpha}, v_F, \tilde{h}_2) \equiv \left(\frac{1}{3\tilde{\alpha}}\right)^{\nu_{k_F}+2} \frac{1}{8} C_0^3 \frac{(2\nu_{k_F} + 1) \left(\frac{1}{2\sqrt{3}}\tau + \nu_{k_F} - \frac{\sqrt{3}}{4}\right) \Gamma(\tau + \nu_{k_F} + \frac{3}{2})^2 \Gamma(\tau + \nu_{k_F} - \frac{1}{2})^2}{\left(\frac{k_F}{\mu} \sqrt{\tilde{\alpha}} + \frac{1}{\sqrt{3}} e_R \sqrt{\tilde{\alpha}}\right) \Gamma(\tau - 1)^2}, \quad (\text{V.79})$$

with

$$\begin{aligned} \nu_{k_F}(e_R, \tau, \tilde{\alpha}) &= \left(\frac{1}{12} \left(\tau - \frac{3}{2}\right)^2 + \frac{k_F^2}{\mu^2} \tilde{\alpha} - \frac{1}{3} e_R^2 \tilde{\alpha}\right)^{\frac{1}{2}} \\ C_0 &= \left(v_F \tilde{h}_2 \sin(\gamma_F + 2\pi\nu_{k_F})\right)^{\frac{1}{1-2\nu_{k_F}}} \\ \gamma_F &= \arg\left(\Gamma(-2\nu_{k_F}) \left(e^{-2\pi i \nu_{k_F}} - e^{-\frac{2\pi}{\sqrt{3}} e_R \sqrt{\tilde{\alpha}}}\right)\right) \end{aligned} \quad (\text{V.80})$$

Note that for a large effective charge $e_R \sqrt{\tilde{\alpha}} \rightarrow \infty$, we have $\gamma_F = -2\pi\nu_{k_F}$ and $C_0 \rightarrow 0$ which implies that the structure function V.78 vanishes in the probe limit $\tilde{\alpha} \sim \frac{N_c}{N_f} \rightarrow \infty$, which is also the regime where the backreaction from the flavor branes can be ignored.

C. R-ratio in the dense regime

The R-ratio for the quantum corrected black hole consists of: 1/ the leading classical contributions (III.22) plus (III.23) both at small and large x respectively; 2/ the sub-leading quantum correction from the emergent Fermi surface (VI.111) in the AdS₂ × R³ in the near horizon approximation; 3/ the sub-leading quantum correction from a normal Fermi liquid far from the horizon in the dilute or probe approximation (VI.113) to be detailed below. To map this ratio on that of a dense nucleus, we follow [13] and define

$$R_{\text{dense}}(x, q^2) \equiv \frac{\frac{1}{A} F_2^{\text{dense}}(x, q^2)}{F_2^{\text{nucleon}}(x, q^2)} \quad (\text{V.81})$$

with the dense structure function

$$\begin{aligned} \frac{F_2^{\text{dense}}(x, q^2)}{A} &\approx \left(C_T \left(\frac{3q^2}{4m_N^2} \right)^{\frac{2}{3}} x^{\frac{1}{3}} + \frac{3C_L}{2x} \left(\frac{3x^2 q^2}{4m_N^2} \right) D(x) \right) \\ &+ \left(C_{\text{AdS}_2} e_R^2 \left(\frac{\mu^2}{q^2} \right)^{\nu_{k_F}+2} x_{k_F}^{\nu_{k_F}+5} (1-x_{k_F})^{\tau-\frac{3}{2}} {}_2F_1^2(\tau_+, \tau_-, \tau-1, 1-x_{k_F}) + \mathbb{C}_1 \frac{F_2^{\text{AdS}_5}(x, q^2)}{A} \right), \end{aligned} \quad (\text{V.82})$$

normalized by the nucleon structure function (VI.114). For clarity, we recap the different definitions used for parton-x ($0 \leq x_A \leq 1$) and entering (V.82) and the normalization (VI.114)

$$\begin{aligned} x_A E_A &= x m_N \\ x m_N &\approx x_{k_F} k_0 \equiv x_{k_F} k_F \end{aligned} \quad (\text{V.83})$$

x_A refers to the parton fraction in a nucleus, x refers to the parton fraction in a nucleon within a nucleus, and x_{k_F} refers to the parton fraction in relation to $k_0 \sim C_0/z_-$ from the emergent Fermi energy.

In (V.82), the first bracket is the leading and classical contribution, and the second bracket is the subleading and quantum contribution. More specifically, the first (III.22) (low-x) and second (III.23) (large-x) contributions stem from DIS scattering on the bulk classical black hole. The third (VI.111) contribution stems from DIS scattering off the emerging holographic liquid close to the black hole horizon. The fourth and last contribution $\frac{F_2^{\text{AdS}_5}(x, q^2)}{A} \equiv \frac{F_2^{\text{dilute}}(x, q^2)}{A}$ (VI.113) stems from DIS scattering off the distorted Fermi liquid far from the horizon in the probe approximation to be discussed thoroughly below. The quantum correction near the black hole is vanishingly small at small-x.

The relative and arbitrary normalization $\mathbb{C}_1 = 0.07$ is introduced to account for the normal Fermi liquid con-

tribution far from the horizon which is asymptotically AdS₅ as we discussed earlier. It will be estimated in the dilute limit below and added to the near horizon contribution. A more quantitative calculation using the exact response function throughout the holographic space distorted by the RN-AdS extremal black hole, that reduces to AdS₂ near the horizon and asymptotes the dilute limit near the boundary, is numerically intensive and goes outside the scope of this work. We note that the values of $\mathbb{C}_1 \leq 0.07$ keep the AdS₂ plus AdS₅ quantum corrections subleading in comparison to the leading RN-AdS black hole contribution for all values of k_F and most parton-x.

To quantify each of the contributions in the R-ratio, we now need to fix the parameters entering this expression, many of which are tied by holography. We first fix the explicit holographic parameters: $\tilde{\alpha} = N_c/4N_f = 1$ (ratio of branes), $2\pi^2 c_5/\sqrt{4\pi\lambda} = 0.01$ (strong coupling) and $e_R = 0.3$ (charge of the probe fermions). Next, we fix the scaling parameters entering in the nucleon pdf: $\tau = 3$ (hard scaling law) and $j = 0.08$ (Pomeron intercept). The nucleon confining scale enters through $\beta = 1/(m_N z_-)^2 \rightarrow \tilde{\beta}$ asymptotically (VI.114). We fix it to $\tilde{\beta} = 17.65$. Finally, we fix the parameters of the emergent Fermi surface: $v_F = 1$ (Fermi velocity), $\tilde{h}_2 = 1$ for simplicity, $\mu/m_N = 1.2$ (chemical potential) for a typical nucleus

With these parameters fixed, we show in Figs. 5-7, the dense R-ratio versus x for different Fermi momenta $k_F/m_N = 4, 0.5, 0.3$. For $k_F/m_N \geq 0.4 \approx k_R/m_N$ the contribution from the emergent AdS₂ Fermi surface near the horizon is small but real. This contribution disappears for $k_F < k_R$ as we noted in (II.11), and only the AdS₅ contribution far from the horizon remains. The contribution from the emergent AdS₂ Fermi surface becomes comparable to the far horizon AdS₅ contribution at large-x and only for large values of k_F/m_N . For all values of k_F/m_N and most values of x , the leading black hole contribution is dominant. Some of the key features

of DIS scattering on a nucleus are already captured by Figs. 5-7 with shadowing and anti-shadowing at small-x due to the coherent scattering on the black-hole, and Fermi motion at large-x that is increasingly apparent from DIS scattering on the AdS₅ from the far horizon part at small k_F/m_N . We will return to these important physical issues below through a more realistic model for DIS scattering on a finite nucleus with comparison to the existing world-data from DIS scattering on light and heavy nuclei.

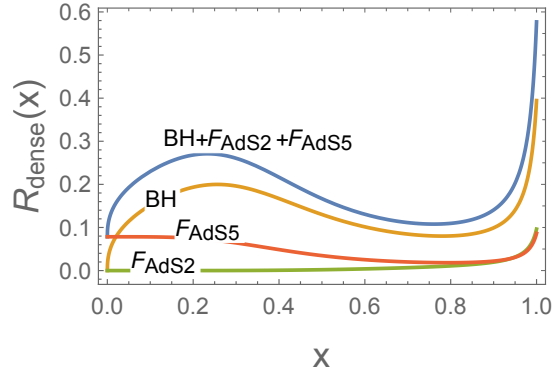


FIG. 5: Dense R-ratio (V.81) with $k_F/m_N = 4$. See text.

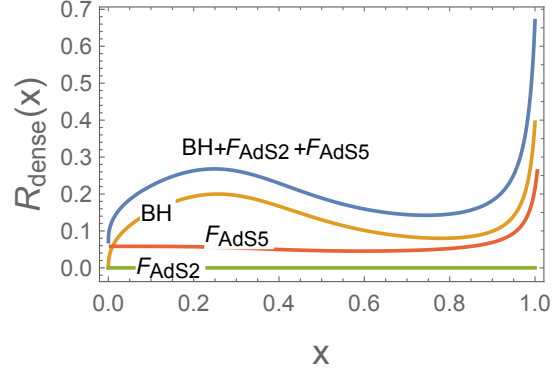


FIG. 6: Dense R-ratio (V.81) with $k_F/m_N = 0.5$. See text.

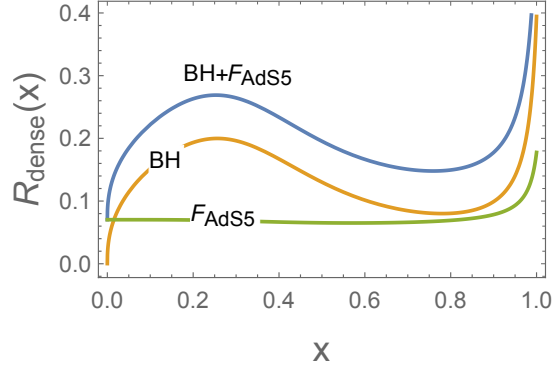


FIG. 7: Dense R-ratio (V.81) with $k_F/m_N = 0.3$, and without the contribution from AdS_2 . See text.

VI. DIS IN THE PROBE LIMIT : DILUTE REGIME

We now consider scattering in the probe limit, where the bulk fermions carry a density without affecting the underlying AdS_5 geometry (with or without a wall), i.e. $\frac{\mu}{\sqrt{\tilde{\alpha}}} \rightarrow 0$ with $\frac{\mu}{\sqrt{\tilde{\alpha}}} \times e_R \sqrt{\tilde{\alpha}} = \mu_e$ fixed where $\tilde{\alpha} \sim \frac{N_c}{N_f} \gg 1$ and μ is the chemical potential. This limit, can be regarded as the UV completion for the emergent Fermi surface in bulk, but also can be considered as DIS scattering

on a very dilute nucleus. This amounts to using the free spectral form (III.31) with the substitution

$$\text{Im} \mathcal{G}_F^{\alpha\gamma}(\omega_1, k) \rightarrow \pi n_F(\omega_1, \vec{k}) \delta(k^2 + \omega_1^2) \delta^{\alpha\gamma} \quad (\text{VI.84})$$

Here $n_F(\omega_1, \vec{k}) = \theta(\mu_e - (k^2 + \omega_1^2)^{\frac{1}{2}})$ is the Fermi occupation factor for a fermion of momentum \vec{k} , mass ω_1 and Fermi energy μ_e , and the vacuum (AdS_5) wavefunctions. For the confining case, the mass ω_1 is quantized. This analysis complements the one we have discussed recently

using generic arguments based on a density expansion of a trapped Fermi liquid [18].

A. Large-x

With this in mind, consider the case of scattering in the ultraviolet region of the black-hole, with the hard

fermion of momentum $k+q$ and the remaining fermion of momentum k treated in the probe approximation. This example will help clarify the relationship between our analysis and that in [21]. For that we use the vacuum propagator (III.30) for both the hard fermion and the density modified propagator (B.6) and (VI.84) for the soft fermion in (III.41),

$$\begin{aligned} \text{Im } \tilde{G}_F^{\mu\nu}(q) &= \int \frac{d^4 k}{(2\pi)^4} \int d\omega_1 \omega_1 \int d\omega_2 \omega_2 \text{Re Tr} \left(\mathcal{G}_F(\omega_1, k+q) \Lambda^\mu(\omega_1; q; \omega_2) \mathcal{G}_F(\omega_2, k) \Lambda^\nu(\omega_2; q; \omega_1) \right), \\ &= \int \frac{d^3 k}{(2\pi)^3} \int_{-|q^0|}^0 \frac{dk^0}{2\pi} \int d\omega_1 \omega_1 \int d\omega_2 \omega_2 \text{Tr} \left(\text{Im } \mathcal{G}_R(\omega_1, k+q) \Lambda^\mu(\omega_1; q; \omega_2) \text{Im } \mathcal{G}_R(\omega_2, k) \Lambda^\nu(\omega_2; q; \omega_1) \right) \end{aligned} \quad (\text{VI.85})$$

where the hard vertices are defined as

$$\begin{aligned} \Lambda^\mu(\omega_1; q; \omega_2) &= \int dr_2 \sqrt{g(r_2)} \bar{\psi}(r_2, \omega_1) Q^\mu(r_2; q) \psi(r_2, \omega_2), \\ \Lambda^\nu(\omega_2; q; \omega_1) &= \int dr_1 \sqrt{g(r_1)} \bar{\psi}(r_1, \omega_2) Q^\nu(r_1; q) \psi(r_1, \omega_1), \end{aligned} \quad (\text{VI.86})$$

Here $\psi(r, \omega)$ and $\bar{\psi}(r, \omega)$ are the hard wave functions [21]

$$\begin{aligned} \psi(z, \omega) &= z^{5/2} [J_{mR-1/2}(\omega z) P_+ + J_{mR+1/2}(\omega z) P_-], \\ \bar{\psi}(z, \omega) &= z^{5/2} [P_- J_{mR-1/2}(\omega z) + J_{mR+1/2}(\omega z) P_+]. \end{aligned} \quad (\text{VI.87})$$

with the chiral projectors $P_\pm = \frac{1}{2}(1 \pm \gamma_5)$. In this regime, the imaginary parts are reducible to on-shell delta functions

$$\begin{aligned} \text{Im } \mathcal{G}_R(\omega_1, k+q) \text{Im } \mathcal{G}_R(\omega_2, k^0, \vec{k}) &\rightarrow \\ &(-(\not{k} + \not{q}) + \omega_1) \pi \delta((k+q)^2 + \omega_1^2) \\ &\times (-\not{k} + \omega_2) \pi n_F(\omega_2, \vec{k}) \delta(k^2 + \omega_2^2) \end{aligned}$$

after using (VI.84). Recall that $n_F(\omega, \vec{k})$ is the Fermi distribution for a fermion of mass ω and momentum \vec{k} near the boundary in the probe limit. With this in mind, (VI.85) becomes

$$\begin{aligned} \text{Im } \tilde{G}_F^{\mu\nu}(q) &\approx \int \frac{d^3 k}{(2\pi)^3} \int_{-|q^0|}^0 \frac{dk^0}{2\pi} \int_0^{q^2} \frac{d\omega_2^2}{2} \int_0^{(q-\omega_2)^2} \frac{d\omega_1^2}{2} \\ &\times \text{tr} \left((-\not{k} + \not{q}) + \omega_1 \right) \Lambda^\mu(\omega_1; q; \omega_2) (-\not{k} + \omega_2) \Lambda^\nu(\omega_2; q; \omega_1) \pi \delta((k+q)^2 + \omega_1^2) \pi \delta(k^2 + \omega_2^2), \\ &= \int \frac{d^3 k}{(2\pi)^3} \int_{-|q^0|}^0 \frac{dk^0}{2\pi} \int_0^{q^2} \frac{d\omega_2^2}{2} \int_0^{(q-\omega_2)^2} \frac{d\omega_1^2}{2} I_{zv}^2(\omega_1, \omega_2, q) \\ &\times \text{tr} \left((-\not{k} + \not{q}) + \omega_1 \right) \gamma^\mu (-\not{k} + \omega_2) \gamma^\nu P_+ \pi \delta((k+q)^2 + \omega_1^2) \pi n_F(\omega_2, \vec{k}) \delta(k^2 + \omega_2^2), \end{aligned} \quad (\text{VI.88})$$

with the physical condition $\omega_1 + \omega_2 < q$ (i.e., a meson or virtual photon of mass q decaying into KK-fermions of

masses ω_1 and ω_2), and

$$\begin{aligned}
I_{zv}(\omega_1, \omega_2, q) &= e_R R^4 q \int_0^\infty dz z^2 J_{mR-1/2}(\omega_1 z) J_{mR-1/2}(\omega_2 z) K_1(qz) \\
&\approx e_R R^4 \frac{2^{-(mR-1/2)}}{\Gamma(mR+1/2)} \omega_2^{mR-1/2} q \int_0^\infty dz z^{mR+3/2} J_{mR-1/2}(\omega_1 z) K_1(qz) \\
&\approx 2e_R R^4 (mR+1/2) \frac{1}{q^2} \left(\frac{\omega_2}{q}\right)^{mR-1/2} \left(\frac{\omega_1}{q}\right)^{mR-1/2} \left(1 + \frac{\omega_1^2}{q^2}\right)^{-(mR+3/2)}
\end{aligned} \tag{VI.89}$$

where we made use of the approximation

$$J_{mR-1/2}(\omega_2 z) \approx \frac{2^{-(mR-1/2)}}{\Gamma(mR+1/2)} (\omega_2 z)^{mR-1/2} \tag{VI.90}$$

for $\omega_2 z \ll 1$. Note that without making the approximation $\omega_2 z \ll 1$, the above integral $I_{zv} \sim$

$F_4(a, b, c, d; -\frac{\omega_1^2}{q^2}, -\frac{\omega_2^2}{q^2})$ [28, 29] where F_4 is the fourth Appell series of hypergeometric functions which is indeed convergent only for $\omega_1 + \omega_2 < q$.

The integral in (VI.89) is in agreement with the R-current scattering on a dilatino in [21]. Evaluating the integral in (VI.88) over ω_1 using the delta-function $\delta(\omega_1^2 - s_k)$, and using (VI.89), we have

$$\text{Im } \tilde{G}_F^{\mu\nu}(q) \approx \frac{\pi}{2} \int \frac{d^3 k}{(2\pi)^3} \int_{-|q^0|}^0 \frac{dk^0}{2\pi} \int_0^{q^2} \frac{d\omega_2^2}{2} I_{zv}^2(\sqrt{s_k}, \omega_2, q) \text{Tr} \left((-\not{k} + \not{q}) + \sqrt{s_k} \gamma^\mu (-\not{k} + \omega_2) \gamma^\nu P_+ \right) \pi n_F \delta(k^2 + \omega_2^2), \tag{VI.91}$$

where $s_k = -(k+q)^2$. The evaluation of the remaining

k^0 -integral in (VI.91) using the last delta-function, yields

$$\text{Im } \tilde{G}_F^{\mu\nu}(q) \approx \frac{\pi}{4} \int_0^{q^2} \frac{d\omega_2^2}{2} \int \frac{d^3 k}{(2\pi)^3} I_{zv}^2(\sqrt{s_k}, \omega_2, q) \text{Tr} \left((-\not{k} + \not{q}) + \sqrt{s_k} \gamma^\mu (-\not{k} + \omega_2) \gamma^\nu P_+ \right) \frac{n_F(\omega_2, \vec{k})}{2E_k}, \tag{VI.92}$$

where $E_k = \sqrt{|\vec{k}|^2 + \omega_2^2} < |q^0|$, and $k^0 = E_k$.

To extract the structure functions (III.17) from (VI.92)

we carry the spin trace by contacting with the time-like frame vector $n^\mu = (1, 0, 0, 0)$,

$$\begin{aligned}
n_\mu n_\nu \text{Im } \tilde{G}_F^{\mu\nu}(q) &\approx \frac{\pi}{4} \int_0^{q^2} \frac{d\omega_2^2}{2} \int \frac{d^3 k}{(2\pi)^3} I_{zv}^2(\sqrt{s_k}, \omega_2, q) \text{tr} \left((-\not{k} + \not{q}) + \sqrt{s_k} \not{n} (-\not{k} + \omega_2) \not{n} P_+ \right) \frac{n_F(\omega_2, \vec{k})}{2E_k}, \\
&\approx \pi \int_0^{q^2} \frac{d\omega_2^2}{2} \int \frac{d^3 k}{(2\pi)^3} I_{zv}^2(\sqrt{s_k}, \omega_2, q) \left((n \cdot k)^2 - \frac{1}{2} (k \cdot q + \sqrt{s_k} \omega_2) n^2 \right) \frac{n_F(\omega_2, \vec{k})}{2E_k},
\end{aligned} \tag{VI.93}$$

where we have assumed $n \cdot q \approx 0$ and $k^2 \approx 0$. Note that

the trace in (VI.93) is the same trace evaluated in [21]

for $\omega_2 = 0$ (see their Eq.72). Using (III.17) with $x_A = -q^2/2P_A \cdot q$, we can now extract the structure functions

$F_{1,2}(x_A, q^2)$ of a state with momentum P_A^μ from (VI.93)

$$\begin{aligned}\tilde{F}_2(x_A, q^2) &\approx 2\pi^2 \frac{q^2}{2x_A (n \cdot P_A)^2} \int_0^{\Lambda^2 < q^2} \frac{d\omega_2^2}{2} \int \frac{d^3k}{(2\pi)^3} I_{zv}^2(\sqrt{s_k}, \omega_2, q) (n \cdot k)^2 \frac{n_F(\omega_2, \vec{k})}{2E_k}, \\ \tilde{F}_1(x_A, q^2) &\approx -\pi^2 \int_0^{\Lambda^2 < q^2} \frac{d\omega_2^2}{2} \int \frac{d^3k}{(2\pi)^3} I_{zv}^2(\sqrt{s_k}, \omega_2, q) (k \cdot q + \sqrt{s_k} \omega_2) \frac{n_F(\omega_2, \vec{k})}{2E_k},\end{aligned}\tag{VI.94}$$

We have $x_k = -q^2/2k \cdot q$, $s_k = -(k+q)^2 \approx -q^2(1-1/x_k)$ and $k^0 = E_k = (|\vec{k}|^2 + \omega_2^2)^{\frac{1}{2}} < |q^0|$. We can reduce

$I_{zv}(\sqrt{s_k}, \omega_2, q)$ in (VI.89) in terms of x_k as

$$I_{zv}(\sqrt{s_k}, \omega_2, q) \approx 2e_R R^4 (mR + 1/2) \omega_2^{mR-1/2} q^{-(mR+3/2)} x_k^{\frac{1}{2}(mR+7/2)} (1-x_k)^{\frac{1}{2}(mR-1/2)}.\tag{VI.95}$$

for the mass range $\omega_2 \leq \Lambda$. Using (VI.95), we can re-write the structure functions (VI.94) in terms of x_k as

$$\begin{aligned}\tilde{F}_2(x_A, q^2) &\approx 2^2 \pi^2 e_R^2 R^8 (\tau - 1)^2 \\ &\times \left(\frac{1}{q^2}\right)^{\tau-1} \frac{1}{x_A (n \cdot P_A)^2} \int_0^{\Lambda^2 < q^2} \frac{d\omega_2^2}{2} (\omega_2^2)^{\tau-2} \int \frac{d^3k}{(2\pi)^3} \frac{n_F(\omega_2, \vec{k})}{2E_k} (n \cdot k)^2 x_k^{\tau+2} (1-x_k)^{\tau-2} \\ \tilde{F}_1(x_A, q^2) &\approx 2\pi^2 e_R^2 R^8 (\tau - 1)^2 \\ &\times \left(\frac{1}{q^2}\right)^{\tau-1} \int_0^{\Lambda^2 < q^2} \frac{d\omega_2^2}{2} (\omega_2^2)^{\tau-2} \int \frac{d^3k}{(2\pi)^3} \frac{n_F(\omega_2, \vec{k})}{2E_k} x_k^{\tau+1} (1-x_k)^{\tau-2},\end{aligned}\tag{VI.96}$$

with the twist parameter is $\tau = mR + 3/2$, following the approximation ($\omega_2 \ll q$)

$$\sqrt{s_k} \frac{\omega_2}{q^2} \approx \left(\frac{1}{x_k} - 1\right)^{\frac{1}{2}} \frac{\omega_2}{q} \approx 0\tag{VI.97}$$

this limit, the graviton exchange Reggeizes by including higher spin- j (stringy) exchange as

$$\mathcal{K}(j, \tilde{q}_0, \tilde{q}_x, z, z') = \int_0^\infty \frac{d\omega^2}{2} \frac{z^2 J_{\tilde{\Delta}(j)}(z\omega) z'^2 J_{\tilde{\Delta}(j)}(z'\omega)}{-t + \omega^2 - i\epsilon}\tag{VI.99}$$

B. Low-x

In contrast to the dense limit in (IV.66), the bulk-to-bulk graviton propagator in the probe limit, is given by

$$G_{xy,xy}(\tilde{q}_0, \tilde{q}_x, z, z') = \int_0^\infty \frac{d\omega^2}{2} \frac{z^2 J_{\Delta}(z\omega) z'^2 J_{\Delta}(z'\omega)}{-t + \omega^2 - i\epsilon}\tag{VI.98}$$

where $t = -\tilde{q}^2 = \tilde{q}_0^2 - \tilde{q}_x^2$. Therefore, $G_{xy,xy}(\tilde{q}_0 = 0, \tilde{q}_x = 0, z, z') \neq 0$ does not vanish in the probe limit. In

with $\tilde{\Delta}(j) = (4 + 2\sqrt{\lambda}(j-2))^{\frac{1}{2}}$.

With this in mind, we now consider the case of the one-loop fermionic contribution in the probe limit at low-x. In this regime, the bulk-to-bulk fermion propagator is of the form [20]

$$D_F(r, r', k) = - \int \frac{d\omega^2}{2} \psi(r) \frac{-i\vec{k} + \omega}{k^2 + \omega^2 - i\epsilon} \bar{\psi}(r')\tag{VI.100}$$

Note that only in this section, we have added an extra factor of i in the gamma matrix in comparison to (III.33) and replaced ω by $-\omega$ to make the comparison with standard results easier. Inserting (IV.64) in

(IV.61), we obtain the on-shell one-loop effective action $\mathcal{S}_F[A_\mu^{(0)} \equiv n_\mu] = n_\mu n_\nu \text{Im} \tilde{G}_F^{\mu\nu}(q)$,

$$\begin{aligned}
n_\mu n_\nu \text{Im} \tilde{G}_F^{\mu\nu}(q) &\approx \int \frac{d^3 k}{(2\pi)^3} \int_{-|q_0|}^0 \frac{dk^0}{2\pi} \int dr \sqrt{-g} \\
&\times \left(n_\mu n_\nu \frac{q^4 R^6}{r^4} [K_0^2(qR^2/r) + K_1^2(qR^2/r)] + q_\mu q_\nu n^2 \frac{q^2 R^6}{r^4} K_1^2(qR^2/r) \right) \\
&\times \text{Tr} \left(\text{Im} D_R(r, r, k) \Gamma^\mu(-ik)_\alpha g^{\alpha\nu} \right) \text{Im} \mathcal{V}_R|_{t=0} \\
&\approx C_\lambda \int dr \sqrt{-g} \sqrt{g^{ii}} g^{ii} \\
&\times \int_0^{q^2} \frac{d\omega^2}{2} \int \frac{d^3 k}{(2\pi)^3} \frac{n_F(\omega, \vec{k})}{2E_k} \left((n \cdot k)^2 \frac{q^4 R^6}{r^4} [K_0^2(qR^2/r) + K_1^2(qR^2/r)] + \frac{q^4}{4x^2} n^2 \frac{q^2 R^6}{r^4} K_1^2(qR^2/r) \right) \\
&\times (\omega R^2/r)^{2mR-1} (R^2/r)^5 \sum_{j=1}^{\infty} \frac{2\sqrt{4\pi\lambda}}{s} (r/R^2)^3 \delta(r - r_j) \\
&\approx C_\lambda \left(\frac{1}{q^2} \right)^{\tau-1} \int_0^{q^2} \frac{d\omega^2}{2} (\omega^2)^{\tau-2} \int \frac{d^3 k}{(2\pi)^3} \frac{n_F(\omega, \vec{k})}{2E_k} \sum_{j=1}^{\infty} \frac{w_j}{2j} w_j^{2\tau+3} \\
&\times \left(\frac{(n \cdot k)^2}{q^2} [K_0^2(w_j) + K_1^2(w_j)] + \frac{1}{4x_k^2} n^2 K_1^2(w_j) \right) \\
&\approx C_\lambda \left(\frac{1}{q^2} \right)^{\tau-1} \int_0^{q^2} \frac{d\omega^2}{2} (\omega^2)^{\tau-2} \int \frac{d^3 k}{(2\pi)^3} \frac{n_F(\omega, \vec{k})}{2E_k} \int_0^\infty dw w^{2\tau+3} \\
&\times \left(\frac{(n \cdot k)^2}{q^2} [K_0^2(w) + K_1^2(w)] + \frac{1}{4x_k^2} n^2 K_1^2(w) \right) \\
&\approx C_\lambda \left(\frac{1}{q^2} \right)^{\tau-1} \int_0^{q^2} \frac{d\omega^2}{2} (\omega^2)^{\tau-2} \int \frac{d^3 k}{(2\pi)^3} \frac{n_F(\omega, \vec{k})}{2E_k} \left(\frac{(n \cdot k)^2}{q^2} [I_{0,2\tau+3} + I_{1,2\tau+3}] + \frac{1}{4x_k^2} n^2 I_{1,2\tau+3} \right)
\end{aligned} \tag{VI.101}$$

Here $E_k = (|\vec{k}|^2 + \omega^2)^{\frac{1}{2}} < |q^0|$, $k^0 = E_k$, and $x_k = -\frac{q^2}{2k \cdot q}$. Also we have set $r_j = R\sqrt{\alpha' s}/2\sqrt{j}$, $w_j = qR^2/r_j = qz_j$,

with $\nu = \frac{1}{2}(n+1)$. They are related to each other recursively $(n-1)I_{1,n} = (n+1)I_{0,n}$.

$$C_\lambda = \frac{\pi c_5 R^4}{2\sqrt{4\pi\lambda}} \frac{2^{-(2mR-1)}}{\Gamma^2(mR+1/2)} \tag{VI.102}$$

and defined the integrals

$$I_{j,n} = \int_0^\infty dw w^n K_j^2(w) = 2^{n-2} \frac{\Gamma(\nu+j)\Gamma(\nu-j)\Gamma(\nu)^2}{\Gamma(2\nu)} \tag{VI.103}$$

The structure functions of the nuclei at small- x in the probe limit are given by

$$\begin{aligned}
\tilde{F}_2(x_A, q^2) &\approx 2\pi C_\lambda \left(\frac{1}{q^2}\right)^{\tau-1} \frac{1}{2x_A (n \cdot P_A)^2} \int_0^{\Lambda^2 < q^2} \frac{d\omega^2}{2} (\omega^2)^{\tau-2} \int \frac{d^3k}{(2\pi)^3} \frac{n_F(\omega, \vec{k})}{2E_k} (n \cdot k)^2 [I_{0,2\tau+3} + I_{1,2\tau+3}] \\
\tilde{F}_1(x_A, q^2) &\approx 2\pi C_\lambda \left(\frac{1}{q^2}\right)^{\tau-1} \int_0^{\Lambda^2 < q^2} \frac{d\omega^2}{2} (\omega^2)^{\tau-2} \int \frac{d^3k}{(2\pi)^3} \frac{n_F(\omega, \vec{k})}{2E_k} \left(\frac{1}{4x_k^2} I_{1,2\tau+3}\right). \tag{VI.104}
\end{aligned}$$

The effects caused by the diffusion in the radial direction on the structure functions far from the black-hole at low-x, are discussed in Appendix E.

C. Normalized structure functions

To normalize the structure functions in the probe limit, we recall that the bulk density and bulk energy density follows from the holographic principle as

$$\begin{aligned}
\tilde{n}(qz \ll 1) &= \int_0^{\Lambda^2} \frac{d\omega^2}{2} I_K(qz \ll 1, \omega) \int_0^{k_F(\omega)} \frac{d^3k}{(2\pi)^3} \\
\tilde{\epsilon}(qz \ll 1) &= \int_0^{\Lambda^2} \frac{d\omega^2}{2} I_K(qz \ll 1, \omega) \\
&\quad \times \int_0^{k_F(\omega)} \frac{d^3k}{(2\pi)^3} \sqrt{k^2 + \omega^2} \tag{VI.105}
\end{aligned}$$

where $k_F(\omega) = \sqrt{\mu_e^2 - \omega^2}$, and

$$\begin{aligned}
I_K(qz \ll 1, \omega) &= R^4 \int_0^{z_-} dz z^{2\tau-3} (\omega^2)^{\tau-2} \\
&= \frac{1}{2} \frac{R^4}{\tau-1} (\omega^2 z_-^2)^{\tau-1} \omega^{-2} \tag{VI.106}
\end{aligned}$$

after taking $qzK_1(qz \ll 1) \approx 1$. The ω -integration in (VI.105) is carried over the bulk spectral density $I_K(0, \omega)$ with an upper cut-off Λ . In the conformal case, the cut-off is a priori arbitrary. In the conformally broken case, say a hard wall at $z = z_-$, we can set $z_- \Lambda = z_- m_N$ in

(VI.105) and assuming Λ large, to pick only the nucleon ground state. A higher cutoff would include higher excited states of the nucleon. With this in mind, we can first undo the k -integration by approximating it near the Fermi surface, and then undo the ω -integration by keeping only the leading contribution for $\frac{1}{\beta} \equiv (z_- m_N)^2 > 1$,

$$\begin{aligned}
\tilde{n}(qz \ll 1) &\approx \frac{1}{8\pi^2} \frac{R^4}{(\tau-1)\beta^{\tau-1}} k_F^3 \\
\tilde{\epsilon}(qz \ll 1) &\approx \frac{1}{8\pi^2} \frac{R^4}{(\tau-1)\beta^{\tau-1}} k_F^3 E_F \tag{VI.107}
\end{aligned}$$

with $E_F = (k_F^2 + m_N^2)^{\frac{1}{2}}$. We now identify the bulk density $\tilde{n} = A/V_A$ as the density of a fixed target say a nucleus, with A -nucleons in a fixed volume V_A and a total energy $E_A = AE_F$. The normalized structure $F_{1,2}$ are then related to our earlier and un-normalized structure functions $\tilde{F}_{1,2}$ through

$$F_{1,2} \equiv 2E_A V_A \tilde{F}_{1,2} = 2AE_A \frac{\tilde{F}_{1,2}}{\tilde{n}} \tag{VI.108}$$

Case-1 (Large-x):

The normalized structure functions at large-x follow by inserting (VI.104) and (VI.107) into (VI.108) with $\beta = 1/(m_N z_-)^2$

$$\begin{aligned}
\frac{F_2(x, q^2)}{A} &\approx 8\pi^2 (\tau-1)^2 e_R^2 \left(\frac{\beta m_N^2}{q^2}\right)^{\tau-1} x_F^{\tau+1} (1-x_F)^{\tau-2} \\
\frac{F_1(x, q^2)}{A} &\approx 4\pi^2 (\tau-1)^2 e_R^2 \left(\frac{\beta m_N^2}{q^2}\right)^{\tau-1} A x_F^{\tau+1} (1-x_F)^{\tau-2}. \tag{VI.109}
\end{aligned}$$

We define the x-fractions

$$\begin{aligned}
x_F &= \frac{q^2}{-2p_F \cdot q} \approx \frac{q^2}{2E_F \omega} = \frac{x m_N}{E_F} \\
x_A &= \frac{q^2}{-2P_A \cdot q} \approx \frac{-q^2}{2E_A \omega} = \frac{x_F}{A} \tag{VI.110}
\end{aligned}$$

and note that the large- x structure functions in (VI.109) in the probe approximation obey the analogue of the Callan-Gross relation $F_2 = 2x_A F_1$ for a holographic and dilute nucleus. Also we note that (VI.109) are analogous to the so-called structure functions of the nucleus obtained through the so-called x -scaling of the structure functions of the nucleon.

Case-2 (Small- x):

Doing the momentum integrals in (VI.104) near $k \rightarrow k_F$ and doing the appropriate normalization as in the large- x regime, we find

$$\begin{aligned} \frac{F_2(x, q^2)}{A} &\approx \pi C_\lambda \left(\frac{\beta m_N^2}{q^2} \right)^{\tau-1} \frac{1}{x_F} [I_{0,2\tau+3} + I_{1,2\tau+3}] \\ \frac{F_1(x, q^2)}{A} &\approx \pi C_\lambda \left(\frac{\beta m_N^2}{q^2} \right)^{\tau-1} A \left(\frac{1}{4x_F^2} I_{1,2\tau+3} \right), \end{aligned} \quad (\text{VI.111})$$

D. R-ratio in the probe limit

We define the R-ratio of the nucleus in the probe (dilute) limit as

$$R_{\text{dilute}}(x, q^2) \equiv \frac{\frac{1}{A} F_2^{\text{dilute}}(x, q^2)}{F_2^{\text{nucleon}}(x, q^2)} \quad (\text{VI.112})$$

where $F_2^{\text{dilute}}(x, q^2)$ is given by the sum of (VI.109) for large- x and (VI.111) for small- x ,

$$\frac{F_2^{\text{dilute}}(x, q^2)}{A} \approx f\left(\frac{\beta m_N^2}{q^2}\right) \times \left(\frac{\beta m_N^2}{q^2}\right)^{\tau-1} \left(8\pi^2(\tau-1)^2 e_R^2 x_F^{\tau+1} (1-x_F)^{\tau-2} + \frac{c_5 \pi^2}{2\sqrt{4\pi\lambda}} \frac{[I_{0,2\tau+3} + I_{1,2\tau+3}]}{2^{(2\tau-4)} \Gamma^2(\tau-1)} \frac{1}{x_F^j} \right), \quad (\text{VI.113})$$

and $F_2^{\text{nucleon}}(x, q^2)$ is given by

$$\frac{F_2^{\text{nucleon}}(x, q^2)}{A} = f\left(\frac{\beta m_N^2}{q^2}\right) \times \left(\frac{\beta m_N^2}{q^2}\right)^{\tau-1} \left(8\pi^2(\tau-1)^2 e_R^2 x^{\tau+1} (1-x)^{\tau-2} + \frac{c_5 \pi^2}{2\sqrt{4\pi\lambda}} \frac{[I_{0,2\tau+3} + I_{1,2\tau+3}]}{2^{(2\tau-4)} \Gamma^2(\tau-1)} \frac{1}{x^j} \right), \quad (\text{VI.114})$$

The additional multiplicative function $f(\iota)$ with argument $\iota = \beta m_N^2/q^2$ asymptotes a constant in the DIS regime which is our AdS₅ result. The specific form of $f(\iota)$ depends on the details of the confining model for finite q^2 (see for example Eq. 3.28 and Eq. 4.3 in [11] for the soft-wall model) but in the DIS limit, the asymptotic constant can be reabsorbed through a shift $\beta \rightarrow \tilde{\beta}$. We recall that $\beta m_N^2 = 1/z_-^2$ is related to the confining scale here, and that $x_F E_F = x m_N$. Also we have in (VI.111) $j = 1$ in the absence of transverse diffusion

or curvature corrections. When the latter are included $j \rightarrow 1 - \mathcal{O}(1/\sqrt{\lambda})$. The structure function of the proton follows from (VI.113) by setting $k_F = 0$ or through the substitution $x_F \rightarrow x$. The R-ratio for the probe or dilute limit is independent of $\beta \rightarrow \tilde{\beta}$ and q^2 . Note that the first contribution is proportional to $e_R^2 \lambda^0$ while the second is proportional to $e_R^0/\sqrt{\lambda}$ independent of the R-charge, as expected for Pomeron-like exchange.

In Fig. 8 we show the behavior of the dilute R-ratio (VI.112) versus x for fixed Fermi momentum $k_F/m_N =$

0.3. The holographic parameters used are fewer but consistent with those used for the dense R-ratio in Fig. 5. Specifically, we have used: $e_R = 0.3$ (R-charge of the bulk fermion), $2\pi^2 c_5/\sqrt{4\pi\lambda} = 0.01$ (strong coupling), $\tau = 3$ (hard scaling exponent), $j = 0.08$ (Pomeron intercept). In the dilute case, the R-ratio is dominant at large- x and asymptotes 1 at small- x . Clearly visible is the EMC-like effect for $0.2 < x < 0.8$ and the Fermi motion for $x > 0.8$. We have checked that the overall features of Fig. 8 remain unchanged for smaller values of e_R but fixed k_F/m_N in conformity with the probe limit. This holographic behavior is very similar to the one we presented recently using general arguments [18].

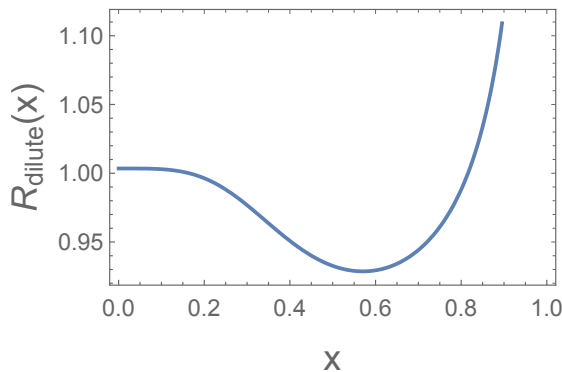


FIG. 8: Dilute R-ratio (VI.112) for $k_F/m_N = 0.3$. See text.

VII. HYBRID MODEL FOR DIS SCATTERING ON A FINITE NUCLEUS

Nuclei to a large extent are a collection of nucleons trapped by a mean-field usually the result of a Hartree-Fock approximation to the two-body and dominant interaction. Three- and higher-body interactions are suppressed as expected from the saturation properties and the bulk compressibility of nuclear matter.

DIS scattering on a nucleus is expected to be dominated by incoherent scattering on a dilute collection of nucleons at intermediate- and large- x , with modifications at small- x due coherent scattering induced by the residual and small two- and three-body mediated interactions following the rapid growth in parton- x .

A way to capture this, short of a more systematic density expansion outlined in [18], is to suggest that the nucleus structure function $F_2^{nucleus}(x, q^2)$ is composed of the dilute contribution (VI.113) warped by AdS₅ (low density and dominant contribution) plus the dense and quantum corrected black-hole (V.82) (high density and subdominant contribution) with a new and arbitrary mixing coefficient \mathbb{C}_2 to be determined from the best fit to the world-data, i.e.,

$$\frac{F_2^{nucleus}(x, q^2)}{A} = \frac{F_2^{dense}(x, q^2)}{A} + \mathbb{C}_2 \frac{F_2^{dilute}(x, q^2)}{A}. \quad (\text{VII.115})$$

The nucleus R-ratio is then

$$R_{nucleus}(x, q^2) \equiv \frac{\frac{1}{A} F_2^{nucleus}(x, q^2)}{F_2^{nucleon}(x, q^2)}. \quad (\text{VII.116})$$

To compare the holographic results following from (VII.116) to the world-data from DIS scattering on heavy and light nuclei, all the holographic parameters are set as before: $\tilde{\alpha} = N_c/4N_f = 1$ (ratio of branes), $2\pi^2 c_5/\sqrt{4\pi\lambda} = 0.01$ (strong coupling) and $e_R = 0.3$ (charge of the probe fermions), $\tau = 3$ (hard scaling law), $j = 0.08$ (Pomeron intercept) and $\beta \rightarrow \tilde{\beta} = 17.65$ (confining scale). The parameters of the emergent Fermi surface are also fixed as before: $v_F = 1$ (Fermi velocity), $\tilde{h}_2 = 1$ for simplicity, $\mu/m_N = 1.2$ (chemical potential for a typical nucleus), and $k_F/m_N = 0.395$ (for Au, Pb, and Fe), 0.277 (for C), 0.119 (for He) (Fermi momentum). We note that our choices for the nuclei Fermi momenta are very close to those extracted from quasielastic electron scattering experiments on nuclei [30] modeled using the Fermi gas model [31]. The parameter $\mathbb{C}_1 = 0.07$ fixes the quantum correction to the black hole due to the far horizon contribution. Our analysis of the data shows that the mixing parameter for the best fit is $\mathbb{C}_2 = 0.793$. Clearly, there is some form of double counting of the quantum corrections at large- x , but this is minimal since $\mathbb{C}_1/\mathbb{C}_2 = 0.09$.

We show in Figs. 9-12a, the nucleus R-ratio versus x for Au, Pb, Fe, C, and He on a linear scale. The overall agreement with the heavy and heavy-light nuclei data is fair throughout, the exception being He where the holographic model overshoots in the anti-shadowing region. This maybe an indication that the coherent scattering captured by the black-hole should be weaker, which is sensible. Figs. 9-12b display the same ratio on a semi-logarithmic scale to highlight the low- x contribution where the data are scarce. A key proposal of the future Electron-Ion-Collider (EIC) is to provide measurements for the nuclear R-ratio in this region.

Remarkably, the R-ratio (VII.116) exhibits shadowing for $x < 0.1$, anti-shadowing for $0.1 < x < 0.3$, the EMC-like effect for $0.3 < x < 0.8$ and Fermi motion for $x > 0.8$. As we noted earlier, shadowing and anti-shadowing are caused by coherent DIS scattering on the dense component in (VII.115) due to the underlying black-hole in our analysis, while the EMC effect and Fermi motion are mostly due to incoherent DIS scattering on the dilute component in (VII.115) with the nucleus mostly composed of individual nucleons warped by AdS₅.

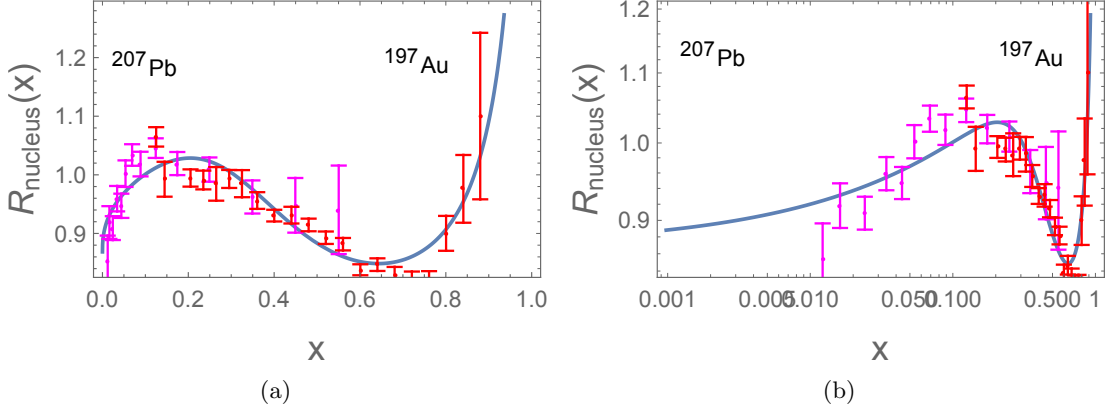


FIG. 9: Nucleus R-ratio (VII.116) for Lead Pb with $A=207$ and Gold Au with $A=197$. We have fixed $k_F/m_N = 0.395$. See text. The data points are from [32, 33] for Pb (pink), and [34] for Au (red), see also Fig.7 in [35].

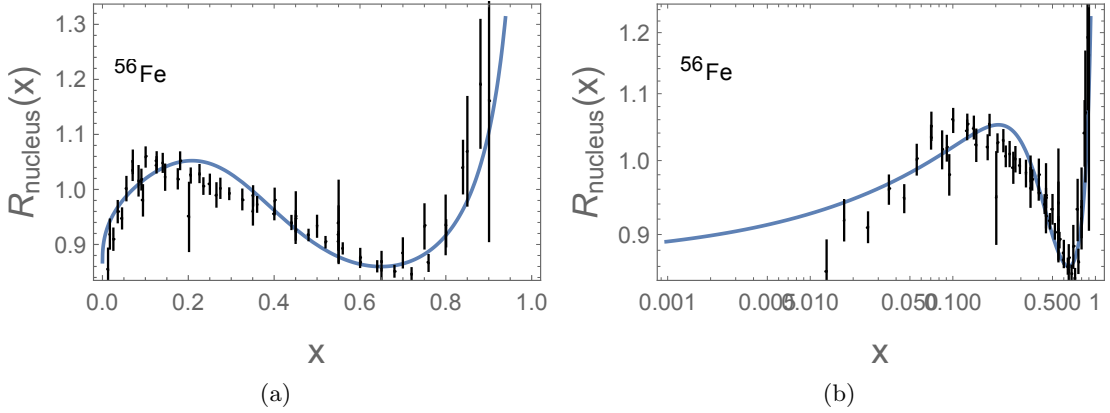


FIG. 10: Nucleus R-ratio (VII.116) for Iron Fe with $A=56$. We have fixed $k_F/m_N = 0.395$. See text. The data points are from [32, 33, 36, 37], see also Fig.5 in [35].

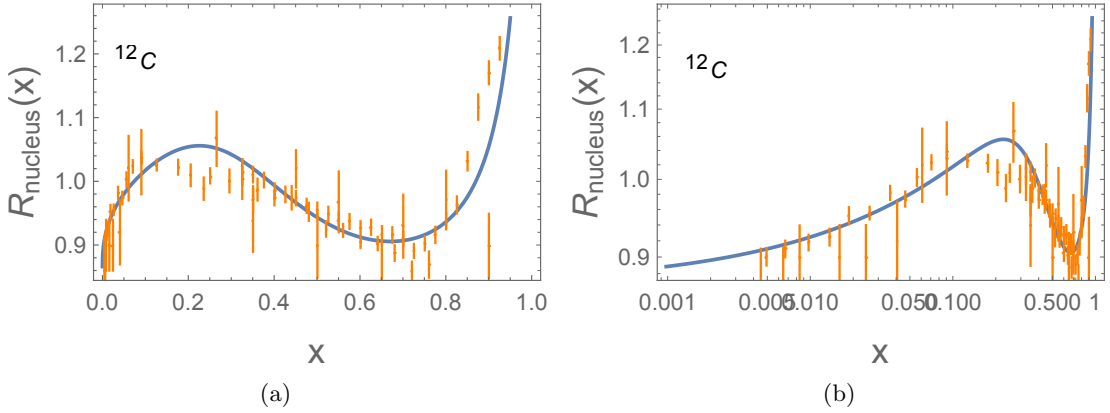


FIG. 11: Nucleus R-ratio (VII.116) for Carbon C with $A=12$. We have fixed $k_F/m_N = 0.277$. See text. The data points are from [34, 38–40], see also Fig.3 in [35].

VIII. CONCLUSIONS

In the double limit of a large number of colors and strong coupling, DIS scattering off an extremal black hole

is of order N_c^2 following from the absorption of the bulk R-current by the black hole. The corresponding struc-

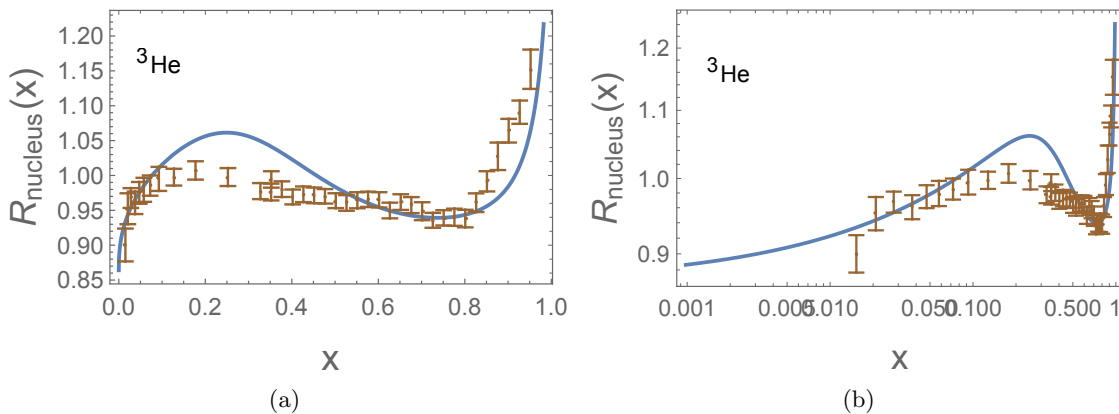


FIG. 12: Nucleus R-ratio (VII.116) for Helium He with $A=3$. We have fixed $k_F/m_N = 0.119$. See text. The data points are from [38, 41], see also Fig.1 in [35].

ture functions are dominated by low- x . Scattering off the black hole is the ultimate coherent scattering off a dense nucleus with strong shadowing as we noted in [13].

To order N_c^0 , DIS scattering is off holographic fermions hovering near the black-hole horizon due to quantum pair creation, and warped holographic fermions far from the black hole horizon near the boundary. Close to the horizon, the geometry is that of $\text{AdS}_2 \times \text{R}^3$ with an emergent Fermi surface and anomalous scaling laws. DIS scattering off these bulk fermions show that their structure functions on the boundary exhibit anomalous exponents and modified hard scattering rules in comparison to scattering off bulk fermions in the dilute or probe limit. DIS scattering off these fermions exhibit Fermi motion at large- x .

DIS scattering on a wide range of nuclei maybe captured by a hybrid holographic model whereby most of the DIS scattering is incoherent and off a holographic Fermi liquid warped by AdS_5 at intermediate- and large- x , with the remainder following from coherent scattering off a quantum corrected RN-AdS black hole at small- x . The ensuing results agree remarkably with the existing data on DIS scattering on finite nuclei over a broad range of parton- x . More data at low- x from the planned EIC collider will be welcome for a better understanding of the coherent scattering through the black-hole mechanism suggested here.

IX. ACKNOWLEDGEMENTS

This work was supported by the U.S. Department of Energy under Contract No. DE-FG-88ER40388.

Appendix A: Conventions in curved space

The gamma matrices in curved and tangent space used to analyze the Dirac equation in the extremal RN-AdS

black hole will be made explicit here. For that, consider the generic line element in curved space

$$ds^2 = -g_{tt}dt^2 + g_{rr}dr^2 + g_{ii}dx_i^2 \quad (\text{A.1})$$

If we refer to the indices in curved space by μ, ν (also t, i) and those in the tangent space by a, b (also $\underline{t}, \underline{i}$) then the gamma matrices are related by

$$\Gamma^\mu = \Gamma^a e_a^\mu, \quad \Gamma^r = \sqrt{g^{rr}} \Gamma^r. \quad (\text{A.2})$$

If we set the vierbeins as [22]

$$e^{\underline{t}} = \sqrt{g_{tt}} dt, \quad e^{\underline{i}} = \sqrt{g_{ii}} dx^i, \quad (\text{A.3})$$

then we have

$$\Gamma^{\underline{t}} = \sqrt{g^{tt}} \Gamma^t, \quad \Gamma^{\underline{i}} = \sqrt{g^{ii}} \Gamma^i, \quad \Gamma^r = \sqrt{g^{rr}} \Gamma^r. \quad (\text{A.4})$$

In the tangent space, the gamma matrices read [17]

$$\begin{aligned} \Gamma^{\underline{t}} &= \begin{pmatrix} i\sigma_1 & 0 \\ 0 & i\sigma_1 \end{pmatrix} & \Gamma^r &= \begin{pmatrix} \sigma_3 & 0 \\ 0 & \sigma_3 \end{pmatrix} \\ \Gamma^{\underline{x}} &= \begin{pmatrix} -\sigma_2 & 0 \\ 0 & \sigma_2 \end{pmatrix} & \Gamma^{\underline{y}} &= \begin{pmatrix} 0 & -\sigma_2 \\ -\sigma_2 & 0 \end{pmatrix} \\ \Gamma^{\underline{z}} &= \begin{pmatrix} 0 & i\sigma_2 \\ -i\sigma_2 & 0 \end{pmatrix}. \end{aligned} \quad (\text{A.5})$$

The non-vanishing spin connections are

$$\omega_{\underline{t}r} = -f_0 e^{\underline{t}}, \quad \omega_{\underline{i}r} = f_1 e^{\underline{i}} \quad (\text{A.6})$$

with

$$f_0 \equiv \frac{1}{2} \frac{g'_{tt}}{\tilde{g}_{tt}} \sqrt{g^{rr}}, \quad f_1 \equiv \frac{1}{2} \frac{g'_{ii}}{g_{ii}} \sqrt{g^{rr}}. \quad (\text{A.7})$$

Appendix B: Soft spinors

The soft normalizable wavefunctions were constructed in [22], we reproduce them here for completeness. The Dirac equation in the $\text{AdS}_2 \times \mathbb{R}^3$ geometry is solved by the rescaled spinors

$$\begin{aligned}\psi_1(r; \vec{k}) &= (-gg^{rr})^{-\frac{1}{4}} \begin{pmatrix} \Phi_1 \\ 0 \\ 0 \end{pmatrix} \times \sqrt{\frac{r_-}{R^2}} \times \left(\frac{r_-}{R^2}\right)^{\nu_k}, \\ \psi_2(r; \vec{k}) &= (-gg^{rr})^{-\frac{1}{4}} \begin{pmatrix} 0 \\ 0 \\ \Phi_2 \end{pmatrix} \times \sqrt{\frac{r_-}{R^2}} \times \left(\frac{r_-}{R^2}\right)^{\nu_k}\end{aligned}\quad (\text{B.1})$$

with

$$\begin{aligned}\Phi_1 &= \begin{pmatrix} v_1 \\ v_2 \end{pmatrix} \equiv \frac{1}{W} a_+(k_0, k) \Psi_-^{(0)} \\ \Phi_2 &= \begin{pmatrix} \tilde{v}_1 \\ \tilde{v}_2 \end{pmatrix} \equiv \Phi_1(\vec{k} \mapsto -\vec{k})\end{aligned}\quad (\text{B.2})$$

and $W = -iv_+^T \sigma^2 v_-$, $a_+(k_0, k) = \tilde{c}_1(k - k_F) + \tilde{c}_2 k_0 + \dots$, where $\tilde{c}_{1,2} \sim \frac{R^2}{r_-}$. The explicit spinors are

$$\begin{aligned}\Psi_{\pm}^{(0)} &\approx v_{\mp} \left(\frac{r - r_-}{R_2^2}\right)^{\pm \nu_k} \\ v_{\pm} &= \begin{pmatrix} mR_2 \pm \nu_k \\ \frac{kR}{r_-} R_2 + e_R \sqrt{\frac{\tilde{\alpha}}{3}} \end{pmatrix},\end{aligned}\quad (\text{B.3})$$

with $R_2 = R/2\sqrt{3}$, and

$$\nu_k = \sqrt{m_k^2 R_2^2 - \frac{\tilde{\alpha}}{3} e_R^2}, \quad m_k^2 \equiv m^2 + \frac{k^2 R^2}{r_-^2}.\quad (\text{B.4})$$

Note that for pure AdS_2 , the soft wave-functions simplify

$$\Phi_1 = \Psi_-^{(0)} \quad \Phi_2 = \Phi_1(\vec{k} \mapsto -\vec{k}).\quad (\text{B.5})$$

Finally, note that the Feynman propagator for the soft part in (III.34-III.35) is given by

$$D_F(r, r'; k) = \psi_{\alpha}(r, k) \left(\int \frac{d\omega}{2\pi} \frac{\rho_B^{\alpha\gamma}(\omega, \vec{k})}{k^0 - \omega} \right) \overline{\psi}_{\gamma}(r', k)\quad (\text{B.6})$$

with the boundary spectral function $\rho_B(\omega, \vec{k})$, and the normalizable wave function $\psi_{\alpha}(r, \vec{k})$ for the Dirac equation in curved AdS_5 .

Appendix C: Parameters $v_F, h_1, h_2, k_F/\mu$ entering the near horizon Green's function

We recall that the retarded Green's function (II.13) in the near horizon limit can be recast in the form

$$\begin{aligned}\mathcal{G}_R^{11}(k^0, \vec{k}) &\approx \frac{\tilde{h}_1 \mu}{k - \left(\frac{k_F}{\mu}\right) \mu - \frac{1}{v_F} k^0 - \Pi(k^0)} \begin{pmatrix} 0 & 0 \\ 0 & 1 \end{pmatrix} \\ \Pi(k^0) &= \tilde{h}_2 \mu e^{i\gamma_{k_F}} \left(\frac{k^0}{\mu}\right)^{2\nu_k}, \\ \nu_k &= \sqrt{\tilde{\alpha}} \left(\frac{k^2}{\mu^2} - \frac{k_R^2}{\mu^2}\right)^{\frac{1}{2}}, \\ \gamma_k &= \arg \left(\Gamma(-2\nu_k) \left(e^{-2\pi i \nu_k} - e^{-\frac{2\pi}{\sqrt{3}} e_R \sqrt{\tilde{\alpha}}} \right) \right),\end{aligned}\quad (\text{C.1})$$

where $k_R^2/\mu^2 = (e_R^2 \tilde{\alpha} - \frac{1}{4}(\tau - \frac{3}{2})^2)/3\tilde{\alpha}$, and $k_0/\mu \sim C_0/2\sqrt{3}\sqrt{\tilde{\alpha}}$ with the dimensionless constant

$$C_0(\nu_{k_F}) = (v_F \tilde{h}_2 \text{Im}(e^{i\gamma_{k_F}} (-1)^{2\nu_{k_F}}))^{\frac{1}{1-2\nu_{k_F}}}\quad (\text{C.2})$$

The dimensionless parameters v_F , \tilde{h}_1 , \tilde{h}_2 , and k_F/μ that characterize the retarded Green's function (II.13) and (III.35), are in principle determined numerically as in [16] for the 3-dimensional spacetime, and analytically for R-charged black holes as in [17]. Here, we will not carry out the numerical analysis to determine the parameters precisely, but we note that all of them are some functions of e_R , τ , and $\tilde{\alpha}$, i.e., $v_F(e_R, \tau, \tilde{\alpha})$, $\tilde{h}_1(e_R, \tau, \tilde{\alpha})$, $\tilde{h}_2(e_R, \tau, \tilde{\alpha})$, and $k_F/\mu(e_R, \tau, \tilde{\alpha})$. Therefore, the dimensionless parameters v_F , \tilde{h}_1 , \tilde{h}_2 , k_F/μ , and the dimensionful parameter μ are free parameters. The parameter \tilde{h}_1 drops out in the normalization. The remaining parameter is set to $\tilde{h}_2 = 1$ for simplicity.

Appendix D: Effective vertices

The soft-to-hard transition vertices entering in the bulk DIS amplitude involve (B.5) for the reduction to AdS_2 or (B.2) in general for the soft part, with the hard part of the wave-function given by

$$\begin{aligned}u_1 &= \left(\frac{R^2}{r}\right)^{\frac{5}{2}} J_{mR-\frac{1}{2}}\left(\omega_1 \frac{R^2}{r}\right) \\ u_2 &\equiv 0\end{aligned}\quad (\text{D.1})$$

More specifically, for pure AdS_2 , the transition vertex is simply given by

with

$$\Lambda_{11}^x(z_2; \omega_1; q; k) = C(\nu_k) \left(\frac{r_-}{R^2}\right)^{\nu_k + \frac{1}{2}} q \int_0^\infty dz_2 z_2^{\frac{3}{2} + \nu_k} K_1(qz_2) J_{mR - \frac{1}{2}}(\omega_1 z_2), \quad (\text{D.2})$$

$$C(\nu_k) = e_R R^2 (mR_2 + \nu_k) (2\sqrt{3})^{-\nu_k}. \quad (\text{D.3})$$

In general, the transition vertices are of the form

$$\begin{aligned} \Lambda_{11}^i(r_2; \omega_1; q; k) &= -e_R \left(\frac{r_-}{R^2}\right)^{\nu_k + \frac{1}{2}} \int dr_2 \sqrt{-g} (-gg^{rr})^{-\frac{1}{4}} \sqrt{g^{ii}} K_A(r_2; q) u_1 \begin{pmatrix} 0 \\ 1 \\ 0 \\ 0 \end{pmatrix}^T \Gamma^{\dot{i}} \begin{pmatrix} v_1 \\ v_2 \\ 0 \\ 0 \end{pmatrix}, \\ \Lambda_{22}^i(r_2; \omega_1; q; k) &= -e_R \left(\frac{r_-}{R^2}\right)^{\nu_k + \frac{1}{2}} \int dr_2 \sqrt{-g} (-gg^{rr})^{-\frac{1}{4}} \sqrt{g^{ii}} K_A(r_2; q) u_2 \begin{pmatrix} 0 \\ 0 \\ 0 \\ 1 \end{pmatrix}^T \Gamma^{\dot{i}} \begin{pmatrix} 0 \\ 0 \\ \tilde{v}_1 \\ \tilde{v}_2 \end{pmatrix}, \\ \Lambda_{11}^j(r_1; k; q; \omega_1) &= -e_R \left(\frac{r_-}{R^2}\right)^{\nu_k + \frac{1}{2}} \int dr_1 \sqrt{-g} (-gg^{rr})^{-\frac{1}{4}} \sqrt{g^{jj}} K_A(r_1; q) u_1 \begin{pmatrix} v_1 \\ v_2 \\ 0 \\ 0 \end{pmatrix}^T \Gamma^{\dot{j}} \begin{pmatrix} 0 \\ 1 \\ 0 \\ 0 \end{pmatrix}, \\ \Lambda_{22}^j(r_1; k; q; \omega_1) &= -e_R \left(\frac{r_-}{R^2}\right)^{\nu_k + \frac{1}{2}} \int dr_1 \sqrt{-g} (-gg^{rr})^{-\frac{1}{4}} \sqrt{g^{jj}} K_A(r_1; q) u_2 \begin{pmatrix} 0 \\ 0 \\ \tilde{v}_1 \\ \tilde{v}_2 \end{pmatrix}^T \Gamma^{\dot{j}} \begin{pmatrix} 0 \\ 0 \\ 0 \\ 1 \end{pmatrix}. \end{aligned} \quad (\text{D.4})$$

Using the gamma matrices explicitly, we can simplify the effective vertices (D.4). More specifically, we have

$$\begin{aligned} \Lambda_{11}^x(r_2; \omega_1; q; k) &= ie_R \left(\frac{r_-}{R^2}\right)^{\nu_k + \frac{1}{2}} \\ &\times \int dr_2 \sqrt{-g} (-gg^{rr})^{-\frac{1}{4}} \sqrt{g^{xx}} K_A(r_2; q) u_1 v_1, \end{aligned} \quad (\text{D.5})$$

$$\begin{aligned} \Lambda_{11}^x(z_2; \omega_1; q; k) &= C(\nu_k) a_+(k_0, k) I_z(\omega_1; q; k) \\ &= C(\nu_k) a_+(k_0, k) \left(\frac{r_-}{R^2}\right)^{\nu_k + \frac{1}{2}} \\ &\times \int_0^\infty dz_2 z_2^{\frac{3}{2} + \nu_k} q K_1(qz_2) J_{mR - \frac{1}{2}}(\omega_1 z_2), \end{aligned} \quad (\text{D.7})$$

with the rest of the vertices following by symmetry

$$\begin{aligned} \Lambda_{11}^x(r_1; k; q; \omega_1) &= -\Lambda_{11}^x(r_2; \omega_1; q; k), \\ \Lambda_{22}^x(r_1; k; q; \omega_1) &= \Lambda_{22}^x(r_2; \omega_1; q; k) \equiv 0, \end{aligned} \quad (\text{D.6})$$

and all other components vanishing. Performing the change of variable $r = R^2/z$ and setting $z \ll z_-$, we can re-write the integral in (D.5) as

with

$$C(\nu_k) = e_R R^2 \frac{(mR_2 + \nu_k)}{W} (2\sqrt{3})^{-\nu_k}, \quad (\text{D.8})$$

The integration can be carried out analytically with the result

$$\begin{aligned}
I_z(\omega_1; q; k) &= \left(\frac{r_-}{R^2}\right)^{\nu_k + \frac{1}{2}} \int_0^\infty dz_2 z_2^{\frac{3}{2} + \nu_k} q K_1(qz_2) J_{mR - \frac{1}{2}}(\omega_1 z_2) \\
&= \left(\frac{r_-}{R^2}\right)^{\nu_k + \frac{1}{2}} C_z(\nu_k) \frac{1}{q^{\nu_k + \frac{3}{2}}} \left(\frac{\omega_1}{q}\right)^{mR - \frac{1}{2}} {}_2F_1\left(\frac{mR + \nu_k + 3}{2}, \frac{mR + \nu_k + 1}{2}, mR + \frac{1}{2}, -\frac{\omega_1^2}{q^2}\right),
\end{aligned} \tag{D.9}$$

with

$$C_z(\nu_k) = 2^{\nu_k + \frac{1}{2}} \frac{\Gamma(\frac{mR + \nu_k + 3}{2}) \Gamma(\frac{mR + \nu_k + 1}{2})}{\Gamma(mR + \frac{1}{2})} \tag{D.10}$$

Note that for the special value $\nu_k = \nu_k^* = mR$, the integrand reduces to the one in [21], and can be evaluated exactly as

$$\begin{aligned}
I_z(\omega_1; q; k) &= \left(\frac{r_-}{R^2}\right)^{\nu_k + \frac{1}{2}} \int_0^\infty dz_2 z_2^{\frac{3}{2} + \nu_k^*} K_1(qz_2) J_{mR - \frac{1}{2}}(\omega_1 z_2) \\
&= \left(\frac{r_-}{R^2}\right)^{\nu_k + \frac{1}{2}} C_z(\nu_k^*, q) q^{-(mR + \frac{5}{2})} \left(\frac{\omega_1}{q}\right)^{mR - \frac{1}{2}} \left(1 + \frac{\omega_1^2}{q^2}\right)^{-(mR + \frac{3}{2})}
\end{aligned} \tag{D.11}$$

and $C_z(\nu_k^*) = 2^{mR + \frac{1}{2}} \Gamma(mR + \frac{3}{2})$.

where [25](see also [26])

Appendix E: Low-x structure functions with radial diffusion

Far from the black hole and including diffusion in the radial direction, the structure functions can be written as

$$\begin{aligned}
F_2(x_A, q^2) &= \int_0^\infty \frac{d\omega^2}{2} \int \frac{d^3k}{(2\pi)^3} \frac{n_F(\omega, \vec{k})}{2E_k} F_2(x_k, q^2, \omega) \\
F_1(x_A, q^2) &= \int_0^\infty \frac{d\omega^2}{2} \int \frac{d^3k}{(2\pi)^3} \frac{n_F(\omega, \vec{k})}{2E_k} F_1(x_k, q^2, \omega),
\end{aligned} \tag{E.1}$$

$$\begin{aligned}
F_2(x_k, q^2, \omega) &= \frac{g_0^2 \rho^{3/2}}{32\pi^{5/2}} \int \frac{dz}{z} \frac{dz'}{z'} P_A^2(z, q^2) P_\psi(z', \omega) (zz' q^2) \frac{e^{\zeta_k(1-\rho)}}{\sqrt{\zeta_k}} e^{-\frac{\log^2(z/z')}{\rho \zeta_k}} \\
2x_k F_1(x_k, q^2, \omega) &= \frac{g_0^2 \rho^{3/2}}{32\pi^{5/2}} \int \frac{dz}{z} \frac{dz'}{z'} P_A^1(z, q^2) P_\psi(z', \omega) (zz' q^2) \frac{e^{\zeta_k(1-\rho)}}{\sqrt{\zeta_k}} e^{-\frac{\log^2(z/z')}{\rho \zeta_k}},
\end{aligned} \tag{E.2}$$

with

$$\begin{aligned}
P_A^2(z, q^2) &= (qz)^2 (K_1^2(qz) + K_0^2(qz)) \\
P_A^1(z, q^2) &= (qz)^2 K_1^2(qz) \\
P_\psi(z', \omega) &= z'^{-3} \times z'^5 J_{mR-1/2}^2(\omega z'),
\end{aligned} \tag{E.3}$$

$\rho \equiv 2/\sqrt{\lambda}$, $\zeta(z, z', \lambda, q^2, x_k) \equiv \log\left(\frac{zz'}{\sqrt{\lambda} x_k}\right)$, and $g_0^2 \equiv \frac{\kappa_5^2}{R^3} = 4\pi^2/N_c^2$.

Appendix F: Black hole with

$$e_R^2 \tilde{\alpha} < \frac{1}{4}(mR)^2 \text{ or } k_R^2 < 0$$

Near the black-hole the bulk fermions get modified in the infrared as illustrated in Fig. 2. The modification depends quantitatively on their charge and mass near the horizon as we discussed earlier. For fermions with $e_R^2 \tilde{\alpha} < \frac{1}{4}(mR)^2$ or $k_R^2 < 0$, the modification is universal

and follows from the reduced $\text{AdS}_2 \times \text{R}^3$ geometry. More specifically, for hard R-probes with large q^0 in the DIS kinematics, only $\mathcal{G}_R(k^0, \vec{k})$ is modified close to the horizon, since $\mathcal{G}_R(\omega_1, k+q)$ carries a large momentum and is mostly unmodified in the ultraviolet. In this regime, the holographic fermions form a disc of radius k_R in momentum space as we noted earlier, with large real and imaginary parts. With this in mind, we have

$$\text{Im } \mathcal{G}_R^{11}(\omega_1, k+q) \text{Im } \mathcal{G}_R^{11}(k^0, \vec{k}) \rightarrow \text{Tr} \left((\sigma_1(k^0 + q^0) - i\sigma_2(k_x + q_x) - \omega_1) \pi \delta((k+q)^2 + \omega_1^2) \times \text{Im } \mathcal{G}_R^{11}(k^0, \vec{k}) \right) \quad (\text{F.1})$$

Here $\mathcal{G}_R^{11} = \mathcal{G}_R \text{diag}(0, 1)$ is given in (II.10) for small ω . Again note the emerging non-Fermi liquid scaling for $\nu_k < \frac{1}{2}$ with the transition to a normal Fermi liquid for

$\omega \approx \omega_c$ as discussed earlier. Using the vertex for pure AdS_2 (D.2), we can re-write (III.41) as

$$\text{Im } \tilde{G}_{xx}^F(q) = q^2 C_\theta (-1) \int_0^\infty \frac{d\omega_1^2}{2} \int dk k^2 C^2(\nu_k) I_z^2(\omega_1; q; k) \text{Re } I_{k^0}(\omega_1, q, x_A), \quad (\text{F.2})$$

with $C_\theta = 1/(12\pi^2)$, and the real part of I_{k^0} is

$$\begin{aligned} \text{Re } I_{k^0}(\omega_1, q, x_A) &= \text{Re} \int_{-\infty}^\infty \frac{dk^0}{2\pi} \text{Tr} \left(\mathcal{G}_F^{11}(\omega_1, k+q) \mathcal{G}_F^{11}(k^0, \vec{k}) \right) \\ &= \text{Re} \int_{-|q^0|}^0 \frac{dk^0}{2\pi} \text{Tr} \left((\sigma_1(k^0 + q^0) - i\sigma_2(k_x + q_x) - \omega_1) \pi \delta((k+q)^2 + \omega_1^2) \text{Im } \mathcal{G}_R^{11}(k^0, \vec{k}) \right) \\ &\approx \int_{-\omega_c}^0 \frac{dk^0}{2\pi} (-1) \omega_1 \pi \delta((k+q)^2 + \omega_1^2) \text{Im } C(\vec{k})(k^0)^{2\nu_k}. \end{aligned} \quad (\text{F.3})$$

By first doing the integral over ω_1 in (F.2) and using the

delta function in (F.3), we finally obtain

$$\begin{aligned}
\text{Im } \tilde{G}_{xx}^F(q) &\approx \frac{C_\theta}{4} \int dk k^2 C^2(\nu_k) q^2 I_z^2(\sqrt{s_k}; q; k) \sqrt{s_k} \text{Im} \left(\frac{-C(\vec{k})(-\omega_c)^{2\nu_k+1}}{2\nu_k+1} \right), \\
&\approx \frac{C_\theta}{4} \left(\frac{1}{q^2} \right)^{\nu_k+\frac{1}{2}} \\
&\times \int dk k^2 C^2(\nu_k) C_z^2(\nu_k) x_k^{\nu_k+5/2} (1-x_k)^{mR-1/2} {}_2F_1^2 \left(\frac{mR+\nu_k+2}{2}, \frac{mR-\nu_k+1}{2}, mR+\frac{1}{2}, 1-x_k \right) \\
&\times \sqrt{s_k} \text{Im} \left(\frac{-C(\vec{k})(-\omega_c)^{2\nu_k+1}}{2\nu_k+1} \right),
\end{aligned} \tag{F.4}$$

with k^0 fixed to ω_c in $s_k = -(k+q)^2$. We have defined $x_k = -q^2/2k \cdot q$, $x_A = q^2/2E_A q_x$, and made use of

the DIS kinematics to approximate $s_k \approx -q^2(1-1/x_k)$, $|q^0| \approx q_x$.

-
- [1] M. R. Adams *et al.* [E665 Collaboration], Phys. Rev. Lett. **68**, 3266 (1992); M. R. Adams *et al.* [Fermilab E665 Collaboration], Phys. Lett. B **287** (1992) 375; M. R. Adams *et al.* [E665 Collaboration], Z. Phys. C **67**, 403 (1995) [hep-ex/9505006].
- [2] P. Amaudruz *et al.* [New Muon Collaboration], Nucl. Phys. B **441**, 3 (1995) [hep-ph/9503291].
- [3] J. Gomez *et al.*, Phys. Rev. D **49**, 4348 (1994).
- [4] A. C. Benvenuti *et al.* [BCDMS Collaboration], Phys. Lett. B **189**, 483 (1987).
- [5] I. Balitsky, Nucl. Phys. B **463**, 99 (1996) [hep-ph/9509348]; Y. V. Kovchegov, Phys. Rev. D **60**, 034008 (1999) [hep-ph/9901281].
- [6] K. J. Golec-Biernat and M. Wusthoff, Phys. Rev. D **59**, 014017 (1998) [hep-ph/9807513].
- [7] C. Adloff *et al.* [H1 Collaboration], Eur. Phys. J. C **13**, 609 (2000) [hep-ex/9908059]; C. Adloff *et al.* [H1 Collaboration], Phys. Lett. B **520**, 183 (2001) [hep-ex/0108035]; C. Adloff *et al.* [H1 Collaboration], Eur. Phys. J. C **21**, 33 (2001) [hep-ex/0012053].
- [8] S. Chekanov *et al.* [ZEUS Collaboration], Eur. Phys. J. C **21**, 443 (2001) [hep-ex/0105090].
- [9] J. Polchinski and M. J. Strassler, JHEP **0305**, 012 (2003) [hep-th/0209211].
- [10] S. J. Brodsky and G. R. Farrar, Phys. Rev. Lett. **31**, 1153 (1973).
- [11] N. R. F. Braga and A. Vega, Eur. Phys. J. C **72**, 2236 (2012) [arXiv:1110.2548 [hep-ph]].
- [12] Y. Hatta, E. Iancu and A. H. Mueller, JHEP **0801**, 063 (2008) [arXiv:0710.5297 [hep-th]].
- [13] K. A. Mamo and I. Zahed, arXiv:1807.07969 [hep-th].
- [14] D. T. Son and A. O. Starinets, JHEP **0603**, 052 (2006) [arXiv:hep-th/0601157]; S. S. Lee, arXiv:0809.3402 [hep-th]; H. Liu, J. McGreevy and D. Vegh, arXiv:0903.2477 [hep-th]; M. Cubrovic, J. Zaanen and K. Schalm, arXiv:0904.1993 [hep-th]; S. J. Sin and I. Zahed, JHEP **0912**, 015 (2009) [arXiv:0907.1434 [hep-th]]; D. T. Son, Phys. Rev. D **78**, 046003 (2008) [arXiv:0804.3972 [hep-th]]; A. Adams, K. Balasubramanian and J. McGreevy, JHEP **0811**, 059 (2008) [arXiv:0807.1111 [hep-th]]; S. S. Gubser and F. D. Rocha, arXiv:0911.2898 [hep-th]. A. Karch, D. T. Son and A. O. Starinets, "Holographic Quantum Liquid," Phys. Rev. Lett. **102**, 051602 (2009); M. Kulaxizi and A. Parnachev, "Holographic Responses of Fermion Matter," Nucl. Phys. B **815**, 125 (2009) [arXiv:0811.2262 [hep-th]].
- [15] A. Chamblin, R. Emparan, C. V. Johnson and R. C. Myers, Phys. Rev. D **60**, 064018 (1999) [arXiv:hep-th/9902170].
- [16] T. Faulkner, H. Liu, J. McGreevy and D. Vegh, Phys. Rev. D **83**, 125002 (2011) [arXiv:0907.2694 [hep-th]].
- [17] S. S. Gubser and J. Ren, Phys. Rev. D **86**, 046004 (2012) [arXiv:1204.6315 [hep-th]].
- [18] K. A. Mamo and I. Zahed, arXiv:1808.01952 [hep-ph].
- [19] L. L. Frankfurt and M. I. Strikman, Phys. Rept. **160**, 235 (1988). R. P. Bickerstaff and A. W. Thomas, J. Phys. G **15**, 1523 (1989); M. Arneodo, Phys. Rept. **240**, 301 (1994).
- [20] J. H. Gao and B. W. Xiao, Phys. Rev. D **81**, 035008 (2010) [arXiv:0912.4333 [hep-ph]].
- [21] J. Polchinski and M. J. Strassler, JHEP **0305**, 012 (2003) [hep-th/0209211].
- [22] N. Iqbal, H. Liu and M. Mezei, arXiv:1110.3814 [hep-th]; T. Faulkner, N. Iqbal, H. Liu, J. McGreevy and D. Vegh, Phys. Rev. D **88**, 045016 (2013) [arXiv:1306.6396 [hep-th]].
- [23] M. Rho, S. J. Sin and I. Zahed, Phys. Lett. B **466**, 199 (1999) [hep-th/9907126]; R. A. Janik and R. B. Peshchanski, Nucl. Phys. B **586**, 163 (2000) [hep-th/0003059]; E. Shuryak and I. Zahed, Annals Phys. **396**, 1 (2018) [arXiv:1707.01885 [hep-ph]].
- [24] R. C. Brower, J. Polchinski, M. J. Strassler and C. I. Tan, JHEP **0712**, 005 (2007) [hep-th/0603115]; A. Ballon-Bayona, R. Carcasses Quevedo, M. S. Costa and M. Djuric, Phys. Rev. D **93**, 035005 (2016) [arXiv:1508.00008 [hep-ph]].
- [25] R. C. Brower, M. Djuric, I. Sarcevic and C. I. Tan, JHEP **1011**, 051 (2010) [arXiv:1007.2259 [hep-ph]].
- [26] N. Kovensky, G. Michalski and M. Schvellinger, JHEP **1810**, 084 (2018) [arXiv:1807.11540 [hep-th]].

- [27] M. Edalati, J. I. Jottar and R. G. Leigh, JHEP **1004**, 075 (2010) [arXiv:1001.0779 [hep-th]].
- [28] L. Y. Hung and Y. Shang, Phys. Rev. D **83**, 024029 (2011) doi:10.1103/PhysRevD.83.024029 [arXiv:1007.2653 [hep-th]].
- [29] D. Jorin, N. Kovensky and M. Schwelling, JHEP **1604**, 113 (2016) [arXiv:1601.01627 [hep-th]].
- [30] E. J. Moniz, I. Sick, R. R. Whitney, J. R. Ficenec, R. D. Kephart and W. P. Trower, Phys. Rev. Lett. **26**, 445 (1971)
- [31] E. J. Moniz, Phys. Rev. **184**, 1154 (1969)
- [32] P. Amaudruz *et al.* [New Muon Collaboration], Nucl. Phys. B **441**, 3 (1995) [hep-ph/9503291].
- [33] M. Arneodo *et al.* [New Muon Collaboration], Nucl. Phys. B **481**, 23 (1996).
- [34] J. Gomez *et al.*, Phys. Rev. D **49**, 4348 (1994).
- [35] S. Malace, D. Gaskell, D. W. Higinbotham and I. Cloet, Int. J. Mod. Phys. E **23**, no. 08, 1430013 (2014) [arXiv:1405.1270 [nucl-ex]].
- [36] A. Bodek *et al.*, Phys. Rev. Lett. **50**, 1431 (1983).
- [37] A. C. Benvenuti *et al.* [BCDMS Collaboration], Phys. Lett. B **189**, 483 (1987).
- [38] J. Seely *et al.*, Phys. Rev. Lett. **103**, 202301 (2009) [arXiv:0904.4448 [nucl-ex]].
- [39] M. Arneodo *et al.* [New Muon Collaboration], Nucl. Phys. B **441**, 12 (1995) [hep-ex/9504002].
- [40] M. Arneodo *et al.* [European Muon Collaboration], Nucl. Phys. B **333**, 1 (1990).
- [41] K. Ackerstaff *et al.* [HERMES Collaboration], Phys. Lett. B **475**, 386 (2000) Erratum: [Phys. Lett. B **567**, 339 (2003)] [hep-ex/9910071, hep-ex/0210067].